1   # Constitutive TRIM22 expression within the respiratory tract identifies

2   # tissue-specific and cell-type dependent intrinsic immune barriers to

3   # influenza A virus infection

4   Matthew Charman[1/2], Steven McFarlane[1], Joanna K. Wojtus[1], Elizabeth Sloan[1], Rebecca

5   Dewar[3], Gail Leeming[4], Mohammed Al-Saadi[4/6], Laura Hunter[5], Miles Carroll[5], James P.

6   Stewart[4], Paul Digard[3], Edward Hutchinson[1]*, & Chris Boutell[1]*.

7

8   [1] MRC - University of Glasgow Centre for Virus Research, Glasgow, G61 1QH, UK

9   [2] Division of Protective Immunity and Division of Cancer Pathobiology, Children's Hospital

10   of Philadelphia, Philadelphia, Pennsylvania, USA

11   [3] The Roslin Institute, University of Edinburgh, Midlothian, EH25 9RG, UK

12   [4] Institute of Infection and Global Health, University of Liverpool, Liverpool, L3 5RF, UK

13   [5] National Infection Service, Public Health England, Porton Down, Salisbury, UK

14   [6] University of Al-Qadisiyah, Al-Qadisiyah, Al-Diwaniyah, Iraq

15

16

17   * Co-corresponding authors: EH: Edward.Hutchinson@glasgow.ac.uk; CB:

18   Chris.Boutell@glasgow.ac.uk

19

20   **Short Title:** TRIM22 confers intrinsic immunity to influenza A viruses

21

Abstract

We hypothesized that increased expression of antiviral host factors at portals of viral entry may protect exposed tissues from the constant threat of invading pathogens. Comparative transcriptomic analysis identified the broad-acting restriction factor TRIM22 (TRIpartite Motif 22) to be among the most abundantly expressed antiviral host factors in the lung, a major portal of entry for many respiratory pathogens. This was surprising, as TRIM22 is currently considered to be an interferon stimulated gene (ISG) product that confers protection following the activation of pathogen-induced cytokine-mediated innate immune defences. Using human respiratory cell lines and the airways of rhesus macaques, we experimentally confirmed high levels of constitutive TRIM22 expression in the lung. In contrast, TRIM22 expression in many widely used transformed cell lines could only be observed following immune stimulation. Endogenous levels of TRIM22 in non-transformed cells were sufficient to restrict human and avian influenza A virus (IAV) infection by inhibiting the onset of viral transcription independently of cytokine-mediated innate immune defences. Thus, TRIM22 confers a pre-existing (intrinsic) tissue-specific immune barrier to IAV infection in the respiratory tract. We investigated whether the constitutive expression of TRIM22 was a characteristic shared by other ISGs in human lung tissue. Transcriptomic analysis identified a large group of ISGs and IAV immuno-regulatory host factors that were similarly enriched in the lung relative to other mucosal tissues, but whose expression was downregulated in transformed cell-lines. We identify common networks of immune gene downregulation which correlated with enhanced permissivity of transformed cells to initiate IAV replication. Our data highlight the importance of tissue-specific and cell-type dependent patterns of pre-existing immune gene expression in the intrinsic intracellular restriction of IAV; findings highly relevant to the immune regulation of many clinically important respiratory pathogens.

47   **Author Summary**

48   The respiratory tract is a major portal of virus entry for many clinically important viruses,

49   including seasonal and pandemic influenza A virus (IAV). We reasoned that cells within the

50   respiratory tract might differentially express antiviral host factors to protect against the

51   constant challenge of viral infection. We found the broad-acting antiviral protein TRIM22,

52   conventionally regarded as an interferon stimulated gene (ISG) product upregulated in

53   response to virus infection, to be constitutively expressed to high levels in the lung. We found

54   that constitutive expression of TRIM22 restricted the initiation of human and avian IAV

55   infection independently of cytokine-mediated innate immune defences. We identified pre-

56   existing tissue-specific and cell-type dependent patterns of constitutive immune gene

57   expression that strongly correlated with enhanced resistance to IAV replication from the

58   outset of infection. Importantly, we show that these constitutive patterns of immune gene

59   expression are lost or downregulated in many transformed cell lines widely used for

60   respiratory virus research. Our data highlight the importance of pre-existing tissue-specific

61   and cell-type dependent patterns of constitutive antiviral gene expression in the intracellular

62   restriction of respiratory viral pathogens not captured in conventional cell culture model

63   systems of infection.

64

65

66

Introduction

Exposure to viral pathogens is a constant threat to all living things and vertebrates have evolved multiple lines of defence to suppress infection. If viruses succeed in penetrating non-specific barrier defences, the activation of pattern recognition receptors (PRRs) by pathogen- and damage-associated molecular patterns (PAMPs and DAMPs, respectively) leads to the activation of innate immune defences, culminating in the secretion of cytokines (including interferons) and the induction of hundreds of interferon stimulated gene (ISG) products [1-4]. ISGs include a wide range of antiviral effectors, and their induced expression from low basal levels to high functional levels plays an important role in limiting viral propagation to resolve pathogen infection [4-6]. However, the induction of this broad antiviral response necessitates pathogen detection by PRRs, which in the case of wild-type influenza A virus (IAV) requires the detection of aberrant viral RNAs (vRNAs) or defective interfering (DI) particles produced during virus replication for optimal induction [1, 3, 7-12]. Accordingly, delayed activation of innate immune defences provides a window of opportunity for viral pathogens to express immunosuppressive genes, which can inhibit or dampen the efficacy of host immune defences [13, 14]. A growing body of evidence suggests that this initial 'gap' in intracellular immunity is covered by intrinsic immunity, also known as intrinsic antiviral resistance or cell autonomous immunity [15-18].

Intrinsic immune effectors are constitutively expressed at levels sufficient to confer protection from the outset of infection. As a result, they can restrict the initiation or progress of viral replication prior to the pathogen-induced activation of PRRs and induction of innate immune defences [15, 16, 19-22]. Notably, many intrinsic antiviral host factors are themselves ISGs (intrinsically expressed ISGs; [18]), which can be further upregulated as a component of the innate immune response upon IFN production. Recent single-cell transcriptomic and reporter-assay studies have provided compelling evidence to support a

92   biological role for intrinsic immunity during IAV infection both *in vitro* and *in vivo*. Cell

93   culture studies have shown individual infected cells of the same lineage to be differentially

94   permissive to IAV infection but to rarely induce the expression of IFN leading to the

95   induction of ISGs [8, 11, 12, 23, 24]. Animal studies have shown lineage-specific patterns of

96   IAV restriction that vary between cell-types, including lung epithelial, fibroblast, endothelial,

97   and resident immune cells [25, 26]. Importantly, these lineage-specific patterns of restriction

98   *in vivo* were shown to occur independently of IRF7 (interferon response factor 7), a critical

99   transcriptional regulator of host innate immune defences to IAV infection [25, 27-32]. These

100   data suggest that intrinsic patterns of constitutive host gene expression are likely to play an

101   important role in limiting IAV replication immediately upon pathogen entry into susceptible

102   host cells, thereby reducing the need to prematurely activate potentially harmful pro-

103   inflammatory innate immune defences [2, 33, 34]. However, evidence for tissue-specific or

104   cell-type intrinsic immune effectors that may restrict IAV replication has remained lacking.

105   We hypothesized that localized intrinsic immune barriers might exist due to tissue-

106   specific patterns of gene expression at common portals of viral entry. We tested this

107   hypothesis in cells derived from the respiratory tract, a major portal of virus entry for many

108   clinically important pathogens, including seasonal and pandemic influenza viruses [35]. In

109   order to identify antiviral genes that might be differentially expressed in the respiratory tract,

110   we initially focused on TRIpartite Motif (TRIM) proteins, a family of over 70 members that

111   participate in a wide range of cellular processes, including multiple aspects of immune

112   regulation and antiviral defence [36-39]. Many TRIM proteins are strongly upregulated in

113   response to IFN signalling and are well established to act as regulators or effectors of innate

114   immunity during virus infection [5, 36-38, 40-45]. Other TRIM proteins are constitutively

115   expressed and known to directly mediate intrinsic immune defences [16, 17, 19, 46-49],

116   including TRIM32 and TRIM41 which have been reported to restrict IAV replication through

117   the targeted degradation of PB1 (polymerase basic protein 1) and NP (nucleoprotein),

118   respectively [21, 22].

119   We focussed particularly on TRIM22, which we identified to be amongst the most

120   abundantly expressed TRIM family members in the respiratory tract. TRIM22 has been

121   implicated in the cellular restriction of a broad range of viruses including

122   encephalomyocarditis virus (EMCV), hepatitis B virus (HBV), hepatitis C virus (HCV),

123   human immunodeficiency virus (HIV), and IAV [50-55]. Studies in transformed cultured

124   cells and primary lymphocytes have shown TRIM22 to be an ISG, strongly upregulated by

125   immune stimuli including type-I (α, β) and -II (γ) IFNs; interleukins (IL-1β, -2 and -15);

126   progesterone and tumour necrosis factor-α (TNF-α) [54-56]. Accordingly, TRIM22 has been

127   shown to inhibit viral infection following its induced expression as an ISG by restricting the

128   onset of viral transcription or by targeted degradation of viral proteins [50-54, 57-60]. With

129   respect to IAV, transient transfection studies in transformed cells have shown TRIM22 to

130   mediate the ubiquitination and proteasome-dependent degradation of NP [55, 61], and to

131   restrict IAV propagation as an effector of the type-I IFN response [55].

132   Here, we show that TRIM22 is constitutively expressed to high levels in the

133   respiratory tract and non-transformed cells of lung origin independently of immune stimulus

134   or viral infection. We demonstrate that the endogenous levels of TRIM22 expression are

135   sufficient to restrict human and avian IAV infection by inhibiting the onset of viral

136   transcription independently of cytokine-mediated innate immune defences. Thus, we identify

137   TRIM22 to confer a pre-existing (intrinsic) intracellular immune barrier to IAV infection

138   within cells of the respiratory airway. Consistent with our hypothesis, these high levels of

139   TRIM22 expression are not present in all cell-types or tissues. Equally importantly,

140   transcriptomic analysis revealed TRIM22 to be amongst a large group of IAV immune

141   regulators that are downregulated in transformed cells which share common networks of

142   immune system disruption correlating with enhanced permissivity to IAV replication.

143   Collectively, our data demonstrate that tissue-specific and cell-type dependent patterns of

144   pre-existing immune gene expression to play a critical role in the intrinsic intracellular

145   restriction of IAV from the outset of infection. These findings are highly relevant to the

146   immune regulation of many clinically important respiratory pathogens.

147

148   **Results**

149   **TRIM22 is constitutively expressed at high levels in the respiratory tract independently**

150   **of immune stimulus or virus infection.**

151   As the respiratory tract is a major portal for virus entry, we hypothesized that cells in the

152   respiratory mucosa might express antiviral proteins to higher levels than cells in less exposed

153   locations, thereby creating localized pre-existing (intrinsic) immune barriers to virus

154   infection. We initially explored this hypothesis using RNA-seq data and protein expression

155   records from Human Protein Atlas (HPA; https://www.proteinatlas.org; [62, 63]) and

156   Genotype-Tissue Expression (GTEx) project (https://gtexportal.org/home/; [64]). We

157   focussed on the TRIM family of proteins, as many members of this family are known to

158   directly or indirectly mediate antiviral immune responses to a wide range of viruses [37]. Of

159   the TRIM family, RNA-seq data from HPA indicated that three members (TRIM8, 22, and

160   28) had the highest transcript expression levels in human lung tissue (Fig 1A, red circles;

161   S1A Table), with TRIM22 being the most abundantly expressed. Notably, expression of these

162   TRIMs was substantially higher than that of TRIM32 and TRIM41, two previously identified

163   intrinsic antiviral regulators of IAV (Fig 1A, blue circles; [21, 22]). TRIM22 transcript levels

164   were most abundantly expressed in the spleen, lymph node, appendix, gallbladder, and lung

165   (Fig 1B, TRIM22 coloured circles; S1B Table), with expression values exceeding the 95%

166   confidence interval for median TRIM22 expression across all tissues. In contrast, transcript

167   levels for both TRIM32 and TRIM41 in the lung were close to their respective median tissue

168   expression values (Fig 1B, TRIM32/41 red circles; S1B Table). Analysis of RNA-seq data

169   obtained by the GTEx project independently confirmed TRIM8, 22, and 28 to be the most

170   abundantly expressed TRIMs in human lung tissue (S1 Fig, S1A Table), with the highest

171   levels of TRIM22 expression observed in the spleen and lung (S1 Fig, S1C Table). Together,

172   these data demonstrate that TRIM22 transcript levels show tissue-specific patterns of gene

173   expression and to be enriched within the lung relative to other tissues or TRIM family

174   members. Analysis of HPA immunohistochemistry (IHC) expression records demonstrated

175   the nasopharynx and bronchus to be among tissues with the highest levels of TRIM22

176   expression (Fig 1C, D). These relatively high levels of tissue-specific protein expression

177   suggest that TRIM22 could make a substantial contribution to a pre-existing and localized

178   intrinsic immune barrier to respiratory airway infection.

179   However, the above data contrast with many previous studies of transformed cultured

180   cells and primary lymphocytes, in which TRIM22 expression is strongly upregulated upon

181   viral infection or immune stimulation [54-56]. To resolve this discrepancy, we first examined

182   how TRIM22 expression in primary human bronchial epithelial (HBEp) cells responded to

183   IFN stimulation. Using a validated TRIM22 antibody (S2 Fig), TRIM22 was readily

184   detectable in unstimulated cells by immunofluorescence (Fig 1E), showing the same

185   predominantly nuclear localisation observed by IHC in respiratory epithelia (Fig 1C). The

186   addition of IFN-β caused an intense upregulation of the ISG Mx1 at both the transcript and

187   protein level. In contrast, TRIM22 expression in the same cells was only increased at the

188   transcript level and not detectably increased at the protein level (Fig 1F-H). We conclude that

189   TRIM22 is constitutively expressed to high levels in non-transformed respiratory epithelial

190   cells independently of immune stimulus. Next, we analysed how TRIM22 expression in the

191   respiratory tract responded to viral infection. As mice lack an orthologue to human TRIM22

192 (https://www.ncbi.nlm.nih.gov/homologene/?term=trim22), we examined tissue from

193 cynomolgus macaques (*Macaca fascicularis*), whose TRIM22 has 92% amino acid identity

194 to human TRIM22. As in human tissue (Fig 1C, D), TRIM22 was constitutively expressed in

195 the respiratory tract of uninfected macaques, specifically in epithelia of the airways, sub-

196 mucosal glands, alveoli, and in alveolar macrophages, with little staining observed in the sub-

197 epithelial connective tissue (Fig 1I, uninfected). In order to determine whether TRIM22

198 expression increased during infection, we compared healthy macaques with those infected

199 with IAV (A/California/04/2009 (H1N1); Cal). These macaques had previously been shown

200 to be infected and to be undergoing an induced innate immune response at the point of

201 euthanasia [65]. Automated staining and quantitation of sectioned samples demonstrated

202 TRIM22 expression did not increase in the respiratory tract of IAV infected macaques (Fig

203 1I, J). In contrast to its expression as an ISG in other settings [54, 55], these data demonstrate

204 that the high levels of constitutive TRIM22 expression observed in primary HBEp cells is

205 representative of its expression profile in the epithelium of the respiratory tract independently

206 of immune stimulation.

207

208 **Constitutive TRIM22 expression correlates with low permissivity to IAV infection.**

209 We next wished to investigate the antiviral properties of constitutively expressed TRIM22.

210 However, while we could demonstrate strong constitutive expression of TRIM22 in HBEp

211 cells, these primary cells are challenging to maintain at high densities for functional studies

212 due to the rapid onset of cellular senescence. Accordingly, to identify a tractable cell line that

213 maintained constitutive expression of TRIM22, we screened a panel of human cell lines for

214 TRIM22 transcript and protein expression levels with and without IFN-β stimulation. In all

215 virally-transformed cell lines examined (HEK 293T, HeLa, HEp2, and A549), TRIM22 was

216 either absent or, as observed for the ISG Mx1, only detected following IFN-β stimulation

217   (Fig 2A-D, S3 Fig). Thus, IAV infection studies that have utilize transformed cell lines would

218   not capture the endogenous antiviral properties of TRIM22 observed at the site of natural

219   infection (Fig 1; [55, 61]). In contrast, both primary and human telomerase reverse

220   transcriptase (hTERT)-immortalized human lung fibroblasts (MRC5 and MRC5t,

221   respectively) retained constitutive expression of TRIM22 independently of IFN-β stimulation

222   (Fig 2A-D, S3 Fig). As single-cell transcriptomics experiments have shown lung fibroblasts

223   to be susceptible to IAV infection *in vivo* [25], we chose MRC5t cells as a model cell line to

224   study the effects of constitutive TRIM22 expression on respiratory virus infection.

225   In order to investigate whether patterns of TRIM22 expression correlated with

226   permissivity to IAV infection, we carried out IAV infections in a panel of cells with different

227   TRIM22 expression phenotypes: constitutive (MRC5 and MRC5t), interferon-inducible

228   (A549), or absent (HEK 293T). First, to determine if constitutive TRIM22 expression

229   correlated with a block to viral entry, cells were infected with IAV (A/Puerto Rico/8/1934

230   (H1N1); PR8) at a multiplicity of infection (MOI) of 1 PFU/cell (based on titres derived in

231   MDCK cells) in the presence of cycloheximide to prevent viral protein synthesis and genome

232   replication. Similar levels of genome segment 7 (Seg. 7) vRNA were detected in the nuclei of

233   infected cells at 2 hours post-infection (hpi) independently of cell lineage, indicating that all

234   cells were equally permissive to viral entry and genome translocation to the nucleus (Fig 2E,

235   F). Next, we tested whether TRIM22 expression patterns correlated with an inhibition of viral

236   replication. To do this we compared the plaque titre of IAV (A/WSN/33 (H1N1); WSN) in

237   each cell type to that in MDCK cells. IAV formed plaques in A549 and HEK 293T cells with

238   an efficiency approximately equal to that in MDCK cells. In contrast, plaque formation in

239   MRC5 and MRC5t cells was strongly suppressed (80 to 100-fold relative to MDCK cells; Fig

240   2G). The correlation of constitutive TRIM22 expression with restricted IAV plaque

241   formation in both MRC5 and MRC5t cells suggested that constitutive TRIM22 expression

242   may confer a pre-existing (intrinsic) intracellular immune barrier to IAV replication.

243

244   **Constitutively expressed TRIM22 restricts the initiation of IAV replication.**

245   In order to examine in more detail how TRIM22 expression patterns influenced permissivity

246   to IAV infection, we focussed on MRC5t cells, in which TRIM22 is constitutively expressed,

247   and A549 cells, in which TRIM22 is an ISG (Fig 2A). First, we compared patterns of

248   TRIM22 expression during IAV (WSN) infection. In MRC5t cells, TRIM22 showed similar

249   levels of constitutive expression both before and during a single-cycle of infection (up to 8

250   hpi; MOI of 1 PFU/cell based on MRC5t titres). In contrast, TRIM22 was barely detectable

251   in A549 cells under equivalent infection conditions, as was the ISG Mx1 (Fig 3A). TRIM22

252   and Mx1 were only detectable in A549 cells following multi-cycle replication (48 hpi; MOI

253   of 0.01 PFU/cell based on A549 titres), indicative of the induction of innate immune defences

254   and ISG expression in response to PAMPs (aberrant vRNAs and DI particles) produced

255   during viral replication (Fig 3B; [1, 11]).

256   Next, in order to identify the specific effects of TRIM22 we generated stable MRC5t

257   and A549 cell lines expressing non-targeting control and TRIM22-targeting short hairpin

258   RNAs (shCtrl and shTRIM22, respectively). The expression of *TRIM22* mRNA in MRC5t

259   shTRIM22 cells was substantially depleted relative to control cells (Fig 3C, S2 Fig). As a

260   result, the expression of TRIM22 protein was significantly knocked down in both MRC5t and

261   A549 cells, with or without IFN-β stimulation (Fig 3D, E). To identify the contribution of

262   TRIM22 to the cellular restriction of IAV replication, we infected these cells with IAV

263   (WSN) at a low MOI (0.001 PFU/cell based on titres relative to each parental cell line) and

264   used MDCK plaque assays to measure the release of infectious virus into the growth media

265   over time. Depletion of TRIM22 enhanced IAV replication in both MRC5t and A549 cells

266 relative to their respective controls, confirming the ability of TRIM22 to restrict IAV

267 replication (Fig 3F; [55]); a phenotype attributable in A549 cells to the ISG induction of

268 TRIM22 during multi-cycle replication (Fig 3B; [55]). We next examined the relative plaque

269 titre of IAV in TRIM22 depleted cells compared to that in their respective control cell lines,

270 reasoning that the ability of the virus to form plaques in these cells would reflect the ability of

271 constitutively expressed TRIM22 to restrict IAV replication from the outset of infection. We

272 infected cells with serial dilutions of IAV (WSN) and counted the number of plaques formed

273 by 36 hpi (Fig 3G). In MRC5t cells, depletion of TRIM22 significantly enhanced the plaque

274 titre of IAV. In contrast, depletion of TRIM22 in A549 cells had no significant effect (Fig

275 3H). We conclude that the constitutive expression of TRIM22 in non-transformed respiratory

276 cells confers a pre-existing immune barrier to IAV infection that restricts viral replication

277 leading to plaque formation.

278

279 **Constitutively expressed TRIM22 provides broad protection against IAV independently**

280 **of the IFN response.**

281 Even though TRIM22 is constitutively expressed in MRC5t cells, it could act to restrict IAV

282 infection by modulating innate immune signalling pathways, a widespread mode of action

283 among the TRIM family [37, 45]. If this was the case, TRIM22 might be required to

284 potentiate an innate antiviral immune response, but not provide a direct intracellular barrier to

285 infection itself. To examine this, we tested the effects of TRIM22 in the presence of the Janus

286 associated kinase (JAK) inhibitor Ruxolitinib (Ruxo), which has been shown to inhibit the

287 induction of cytokine-mediated innate immune defences and ISG expression in response to

288 IAV infection [66]. We first determined a concentration of Ruxo that would block ISG

289 induction (*Mx1* and *ISG15*) in MRC5t cells following IFN-β treatment (Fig 4A; 4 μM).

290 Comparing the effects of Ruxo (4 μM) or DMSO (carrier control) treatment on the relative

291   plaque titre of IAV in TRIM22 depleted or control MRC5t cells showed that TRIM22

292   depletion caused the same increase in relative plaque titre regardless of the inhibition of JAK-

293   STAT signalling (Fig 4B). Thus, constitutively expressed TRIM22 restricts IAV replication

294   independently of pathogen-induced cytokine-mediated innate immune defences.

295   As WSN is a highly laboratory-adapted strain, we tested whether constitutively

296   expressed TRIM22 was effective against other IAV strains using an immunofluorescent

297   focus-forming assay to measure the proportion of IAV NP positive cells at 8 hpi. Depletion

298   of TRIM22 increased the focus-forming efficiency of a panel of influenza A viruses,

299   including two avian strains (Fig 5A, B). Thus, constitutively expressed TRIM22 provides a

300   broad-acting intrinsic immune barrier to IAV that restricts NP expression, protecting non-

301   transformed respiratory cells against human and avian IAV from the outset of infection.

302

303   **TRIM22 provides intrinsic immunity against IAV by limiting the onset of viral**

304   **transcription.**

305   Having established that the constitutive expression of TRIM22 confers a pre-existing intrinsic

306   immune barrier to IAV, we wished to determine the point in viral replication at which it

307   acted. We infected TRIM22 depleted or control MRC5t cells with IAV (PR8; MOI of 0.05

308   PFU/cell based on titres derived from MRC5t cells) in the presence of cycloheximide to

309   inhibit viral protein synthesis and genome replication. Nuclei were isolated at 4 hpi and the

310   relative levels of input vRNA were quantified by qRT-PCR. Western blotting for histone H3

311   and actin confirmed successful cell fractionation (Fig 6A). TRIM22 depletion did not

312   significantly alter the nuclear accumulation of IAV genomes (Fig 6B), demonstrating that

313   constitutive TRIM22 expression was not a barrier to viral genome entry into the nucleus of

314   infected cells.

315   We next asked whether TRIM22 might affect the stability of incoming viral genomes

316   via degradation of NP, as transient transfection studies in HEK 293T cells have shown

317   TRIM22 to target NP for ubiquitination and proteasome-mediated degradation [55, 61].

318   However, we were unable to detect any alteration of NP accumulation caused by TRIM22 in

319   HEK 293T cells using an equivalent assay (Fig 6C, D). Nor were we able to detect any

320   difference in genome stability between TRIM22 depleted or control MRC5t cells within the

321   first four hours of IAV infection, prior to the onset of viral genome replication (Fig 6B and

322   Fig 6E, 0 to 4 hpi). Thus, endogenous levels of constitutive TRIM22 expression can restrict

323   IAV replication without influencing the stability of incoming viral ribonucleoproteins

324   (vRNPs). However, following the onset of *de novo* vRNA synthesis higher levels of vRNA

325   accumulated in TRIM22 depleted cells compared to control cells (Fig 6E, 4 to 8 hpi). These

326   data suggested that endogenous TRIM22 affects viral genome replication. In order to

327   replicate, IAV genomes must be encapsidated by newly synthesized viral proteins [35]. We

328   therefore used qRT-PCR and western blotting to measure the transcription and expression

329   profiles of the viral NP, M1 and NS1 genes, each encoded by independent genome segments,

330   over a time course of infection. TRIM22 depletion increased transcription of all three genes

331   (Fig 6F), correlating in each case with an increase in viral protein synthesis (Fig 6G, H).

332   While transcription and replication of the IAV genome are intimately linked, the differences

333   in mRNA levels were detectable prior to differences in *de novo* vRNA synthesis under

334   equivalent infection conditions (Fig 6E, F). Thus, TRIM22 provides intrinsic immunity to

335   IAV infection by suppressing the onset of viral transcription to restrict, either directly or

336   indirectly, the initiation of viral genome replication. Collectively, these data highlight that

337   constitutively expressed TRIM22 inhibits IAV replication early in the infectious cycle (2 to 4

338   hpi; Fig 6F) prior to the accumulation of viral immuno-evasion genes (for example NS1, Fig

339   6G, H; [13, 14]).

340

Human lung tissue is enriched for constitutive ISG expression.

342   Having identified TRIM22 to be a constitutively expressed ISG product within the

343   respiratory tract that confers protection to IAV infection (Fig 1, 3, 5), we next examined

344   whether other ISGs were constitutively expressed to high levels in the lung relative to other

345   mucosal (gastrointestinal tract; esophagus, colon, and small intestine) or non-mucosal (liver,

346   skin, and kidney) tissues. Using GTEx project (https://gtexportal.org/home/; [64]) RNA-seq

347   data obtained from human tissue biopsies, we examined the transcript expression profiles of

348   200 ISGs previously identified to be upregulated in response to universal IFN stimulation in

349   primary cell culture ($\geq$ 8-fold change; [67]) (Fig 7, S2A Table). This analysis showed that

350   individual tissues expressed distinct profiles of ISG transcript expression (Fig 7A, ranked by

351   lung expression), with TRIM22 amongst the top 50 most abundantly expressed ISGs in the

352   lung (Fig 7B, ranked by lung expression). Significantly higher levels of median ISG

353   transcript expression were observed in the lung relative to all other tissues examined (Fig 7C,

354   200 ISGs). Principle component analysis (PCA) and clustering demonstrated that individual

355   ISGs were not equally expressed in all tissues (Fig 7D), with lung tissue sharing the highest

356   degree of ISG profile similarity to that of the small intestine (Fig 7E). Transcript levels of

357   type-I (α, β), -II (γ), and -III (λ) IFNs were either not detectable or extremely low ($\leq$ 1.3

358   TPM; Fig 7F, G, S2B Table), indicating that ISG enrichment in these tissues occurred

359   independently of high levels of constitutive IFN transcription. While a role for IFN in the

360   tissue-dependent enrichment of specific ISGs cannot be ruled out [18, 68, 69], these data

361   demonstrate the existence of tissue-specific profiles of constitutive ISG transcription and

362   show that lung tissue is enriched in ISG transcripts relative to other tissues.

363   Notably, many well established antiviral ISGs (BST2, IFITM1, and SAMHD1) and

364   IAV associated host restriction factors, including the GBP (guanylate-binding protein)

365   family, were observed to have high levels of constitutive ISG transcript expression in the

366   lung (Fig 7B) [70, 71]. These data suggest that enriched levels of pre-existing ISG expression

367   in the lung may combine to confer enhanced antiviral protection against respiratory airway

368   infection immediately upon pathogen entry into susceptible host cells.

369

370   **The disruption of intracellular immune networks in transformed cells increases**

371   **permissivity to IAV replication.**

372   Since the constitutive expression of TRIM22 is lost in many transformed cell lines (Fig 2A-

373   D, S3 Fig), we hypothesized that other constitutively expressed ISGs might also be

374   downregulated. Using cell-line RNA-seq data sets obtained from HPA

375   (https://www.proteinatlas.org; [62, 63]), we compared the ISG transcript expression profile of

376   non-treated hTERT-immortalized human bronchial epithelial cells (HBEC3-KT; HBEC3) to

377   that of three widely used transformed cell lines (A549, HEK 293, and HeLa). Out of the 200

378   ISGs previously examined (Fig 7A), 178 ISGs were identified in RNA-seq cell line data sets

379   (S3A Table) with 87 ISGs having values $\geq$ 5 TPM (Fig 8A; median 3.5 TPM per gene across

380   all cell lines). Relative to HBEC3 cells, many of these ISGs were downregulated in

381   transformed cells in an ISG-specific and cell-line dependent manner (Fig 8B; HBEC3 $\geq$ 5-

382   fold change). Out of the 34 ISGs identified to be differentially downregulated in transformed

383   cells (S3B Table), several were downregulated in all three (defined as core) or in two

384   (defined as shared) transformed cell lines (Fig 8B, C). Importantly, the profile of ISG

385   expression in unstimulated HBEC3 cells for this subset of ISGs was similar to that observed

386   in lung tissue (Fig 8B; 34 ISGs); although the overall ISG expression profile significantly

387   varied between lung tissue and all cell lines examined (S4 Fig; 178 ISGs). Network analysis

388   using STRING (https://string-db.org; [72]) demonstrated that many of these downregulated

389   ISGs were connected in the immune system network (17 of 34 genes; Fig 8C, D), and as a

390   gene set to show pathway enrichment for defence response to virus and IAV infection (Fig

391   8D). Collectively, these data demonstrate that transformed cells display lineage-specific

392   patterns of constitutive ISG expression, with a significant number of ISGs being

393   downregulated relative to HBEC3 cells or lung tissue.

394   Having identified a subset of constitutively expressed ISGs known to restrict IAV to

395   be downregulated in transformed cells (Fig 8), we extended our analysis to determine

396   whether other immune system-related genes were downregulated relative to HBEC3 cells

397   (HBEC3 ≥ 5-fold change; blue circles in Fig 9A; S4A Table). Gene Ontology (GO) analysis

398   identified that a significant percentage of differentially downregulated genes in A549

399   (18.09%), HEK 293 (17.39%), and HeLa (16.46%) cells map to the immune system (S4B, C

400   Tables). Out of the 174 unique immune genes identified to be downregulated, 95 (54.6%)

401   were common to at least two transformed cell lines (Fig 9B, core + shared; S4D Table).

402   STRING analysis identified a significant degree of network connectivity between these

403   downregulated immune genes (141 of 174 genes; Fig 9C, S5 Fig), with common (core +

404   shared) immune genes located across the entire network. We conclude that transformed cells

405   share common networks of immune system disruption which arise through lineage-specific

406   patterns of immune gene downregulation. Notably, this gene network was also enriched for

407   host factors known to restrict IAV (Fig 9C; KEGG pathway [hsa05164]), suggesting that

408   transformed cells are deficient in multiple host factors known to contribute to the intracellular

409   restriction of IAV.

410   To investigate this observation further, we curated an extended IAV KEGG network

411   which included recently identified host factors that influence IAV restriction (Fig 10A, S5A

412   Table; [70, 71]). Out of the 184 genes analyzed, 39 (21.2%) were identified to be

413   significantly downregulated in transformed cells relative to HBEC3 cells (≥ 5-fold change;

414   Fig 10B, C, S5B Table) or lung tissue. Consistent with both ISG and immune system

415   profiling (Fig 8C, 9B, respectively), many of these genes were downregulated in two or more

416   transformed cell lines and showed significant network connectivity (29 of 39 genes; Fig

417   10D). The expression profiles of a subset of these proteins were tested in unstimulated cells

418   by western blotting, which confirmed that UBA7, TRIM22 (positive control), IFITM1,

419   GBP1, IFIH1 and TLR3 were expressed to significantly lower levels in A549 cells relative to

420   HBEC3 cells (Fig 10E, F). In order to determine if the disruption of this immune system

421   network influenced IAV replication, we compared the relative plaque titre of IAV in HBEC3

422   and A549 cells to that of MDCK cells. Similar to diploid lung fibroblasts (Fig 2G, H), human

423   bronchial epithelial cells were highly restrictive to the initiation of IAV plaque formation

424   relative to MDCK cells ($\geq$ 70-fold) or A549 cells ($\geq$ 30-fold) (Fig 9G, H). Ruxolitinib

425   inhibition of JAK-STAT signalling did not influence the initiation of IAV plaque formation

426   in any of the cell-types examined (Fig 9I), although a significant increase in plaque diameter

427   could be observed in each cell-type (Fig 9J). Thus, pharmacological inhibition of cytokine-

428   mediated innate immune defences enhances virus propagation and spread, but not the

429   initiation of viral replication leading to plaque formation [11, 66]. We conclude that the

430   constitutive expression of IAV immuno-regulatory genes in the context of non-transformed

431   respiratory cells confers a significant pre-existing immune barrier to IAV infection prior to

432   the induction of pathogen-induced cytokine-mediated innate immune defences. Importantly,

433   this intrinsic barrier is compromised in many transformed cell lines currently being used for

434   IAV immunobiology research.

435

436

437

Discussion

439   Recent single-cell transcriptomic studies have identified individual cells to be differentially

440   permissive to IAV infection [24, 25]. These observations suggest that pre-existing (intrinsic)

441   patterns of cellular gene expression within (or between) specific cell-types may differentially

442   influence the outcome of IAV infection. However, biological evidence to support the

443   importance of such cell-type specific patterns of host gene expression in the intracellular

444   restriction of IAV has remained lacking. Consequently, the concept of intrinsic immunity has

445   yet to be firmly accepted within the IAV field or wider respiratory virus research community.

446   Here, we demonstrate that non-transformed human lung cells possess patterns of constitutive

447   antiviral gene expression that differ markedly from the transformed cell culture model

448   systems that have been widely used for respiratory virus research over many decades. We

449   show that these differential patterns of constitutive antiviral gene expression can directly

450   influence the outcome of IAV infection, independently of pathogen-induced cytokine-

451   mediated innate immune defences. Thus, we have identified a biologically important and

452   previously overlooked role for intrinsic immunity in the regulation of IAV infection; findings

453   relevant to the intracellular immune regulation of many respiratory pathogens.

454   Our initial hypothesis that cells in the respiratory mucosa might differentially express

455   antiviral proteins at higher levels than in cells at less exposed locations led to the

456   identification of TRIM22 to be amongst the most abundantly expressed TRIM proteins in

457   lung tissue and non-transformed cells of lung origin (Fig 1, 2A, S1, S6 Fig). This high level

458   of constitutive TRIM22 expression contrasts with many previous studies, which have

459   reported TRIM22 to be strongly upregulated as an effector ISG in primary lymphocytes and

460   transformed cell lines in response to virus infection or immune stimulation (Fig 2, S3 Fig;

461   [54, 55]). We note that TRIM22 (formerly known as Staf50) has been shown to be

462   upregulated by p53 and its expression has been found to correlate with cell differentiation

463   and proliferation status [54, 73]. Thus, the downregulation of constitutive TRIM22

464   expression in many virally-transformed cells may occur as a direct result of p53 inactivation

465   by viral proteins to sustain cellular proliferation. However, it is evident that many

466   transformed and carcinoma cell lines have variable gene copy numbers and an extensive

467   array of single nucleotide polymorphisms (SNPs) that can directly influence cellular protein

468   expression profiles, protein functionality, and immune competence [74-76]. Indeed, analysis

469   of Cancer Cell Line Encyclopaedia (CCLE; [75]) records demonstrate that TRIM22 transcript

470   levels and copy number are downregulated in many lung carcinoma cell-types

471   (https://portals.broadinstitute.org/ccle/page?gene=TRIM22). Such issues of genetic variance

472   raise concerns over the suitability of using carcinoma cells for virus-related immunity studies.

473   For example, it is becoming increasingly evident that many cancers downregulate multiple

474   immune regulators to minimize immune clearance and carry unique epigenetic signatures that

475   influence gene transcriptional regulation and proliferation [74, 75, 77, 78]. Consequently, the

476   utilization of such genetically variable populations of cells for *in vitro* experimentation is

477   likely to have a significant bearing on viral intracellular immune regulation due to lineage-

478   specific patterns of immune gene regulation acquired through transformation.

479   We demonstrate that multiple immune regulators, known to influence the replication

480   of a wide variety of viral pathogens, are downregulated in transformed cell lines widely used

481   for respiratory virus research (Fig 8-10). The loss or downregulation of these constitutively

482   expressed host factors correlates strongly with enhanced permissivity of these cell-types to

483   the initiation of IAV replication leading to plaque formation (Fig 2G, 10H). Many of these

484   immune genes, although downregulated in a lineage-specific manner (Fig 9), share common

485   networks of immune-system regulation known to influence IAV replication (Fig 8C, 9C,

486   10D). These observations may account for much of the gene-specific variability, but

487   interrelated pathway connectedness, observed between genome-wide RNA interference

488   screens that utilized carcinoma model systems to identify host factors that influence IAV

489   replication [79-81]. Collectively, our data highlight the importance of utilizing more

490   physiologically relevant cell culture model systems to improve experimental reproducibility

491   between independent groups and research fields.

492   Using a cell culture system that retained the constitutive expression of TRIM22

493   observed at the natural site of infection (Fig 1, 2), we corroborate previous reports that

494   TRIM22 acts as a restriction factor to inhibit IAV replication (Fig 3F-H; [55, 61]).

495   Importantly, we show that constitutive expression of TRIM22 is sufficient to restrict the

496   initiating cycle of both human and avian IAV replication from the outset of infection by

497   inhibiting the efficient onset of viral transcription (Fig 5, 6). We show that pharmacological

498   inhibition of cytokine-mediated JAK-STAT signalling did not reduce the ability of

499   endogenous TRIM22 to restrict IAV infection (Fig 4; [66]), demonstrating the TRIM22 can

500   work independently of the IFN pathway. Thus, high levels of constitutive TRIM22

501   expression can confer immediate protection to airway infection, thereby reducing the need to

502   prematurely activate potentially harmful pro-inflammatory innate immune defences [2, 33,

503   34].

504   Our work exemplifies two important features of intrinsic immunity. Firstly, we

505   identify TRIM22 to be an intrinsically-expressed ISG, similar to PML (TRIM19) and

506   TRIM5α [19, 46, 48, 49], which can be further upregulated in response to cytokine

507   signalling in a manner dependent on the pre-existing basal levels of endogenous expression in

508   a given cell-type (Fig 1F-H, 2A, B, S3 Fig). Secondly, TRIM22 demonstrates that intrinsic

509   immune defences can be upregulated in a tissue-specific manner. Like TRIM32 and TRIM41

510   [21, 22], TRIM22 can restrict the initiation of IAV infection (Fig 5, 6), but unlike these

511   TRIM proteins TRIM22 is upregulated in a tissue-specific manner, being enriched within the

512   lung relative to other tissues (Fig 1A, B, 7A, B). Collectively, these observations point to a

513   series of distinct ways in which constitutive levels of immune gene expression can influence

514   the outcome of IAV replication independently of pathogen-induced host defences. Further

515   investigation is warranted to determine the accumulative and strain-dependent effects of such

516   intrinsic barriers to IAV infection.

517   We found that constitutively-expressed TRIM22 could restrict the replication of

518   multiple human (H1N1, including WSN) and avian (H3N2 and H7N1) strains of IAV (Fig 5).

519   These data contrast with recent studies in transformed cells [61], which lack constitutive

520   TRIM22 expression (Fig 2A, S3; [55, 61]), that reported the WSN strain to be resistant to

521   TRIM22 mediated restriction. In these studies, TRIM22 was found to target IAV NP for

522   ubiquitination and proteasome-dependent degradation [55, 61], with WSN NP being resistant

523   to ubiquitination due to the substitution of lysine acceptor residues for arginines [61]. In

524   contrast, we found that constitutively-expressed TRIM22 was effective against the WSN

525   strain (Fig 3F-H) independently of detectible NP degradation, either alone or in the context of

526   incoming vRNPs (Fig 6C-E). While we cannot discount a role for ubiquitination in the

527   TRIM22 mediated restriction of IAV, we show endogenous levels of TRIM22 are sufficient

528   to restrict *de novo* NP expression by inhibiting the onset of viral transcription (Fig 5, 6).

529   These differences may reflect cell-type (transformed *vs* non-transformed cells) or expression

530   level (ectopic *vs* endogenous) dependent differences in TRIM22 restriction of IAV and

531   suggest that TRIM22 may adopt multiple approaches to restrict IAV infection. For example,

532   endogenous levels of TRIM22 may sterically hinder the onset of viral transcription

533   independently of NP degradation when in complex with vRNPs, but upon saturation under

534   high genome loads to target *de novo* synthesized free pools of NP for ubiquitination leading

535   to its proteasome-degradation. Such differences in substrate-targeting could result in a switch

536   in intracellular immune 'status' from intrinsic to innate defences, induced by the onset of

537   viral replication or sensing of PAMPs in a strain-dependent manner. Such a mechanism is not

538   unprecedented, as we have recently shown that PML (TRIM19) plays spatiotemporally

539   distinct roles in the regulation of intrinsic and innate immune defences to HSV-1 infection

540   [19, 82]. Further biochemical investigation will be required to determine whether TRIM22

541   has differential modes of substrate-targeting dependent on the kinetics of infection or cellular

542   immune status.

543   A surprising discovery in our study was the identification of enriched levels of

544   constitutive ISG expression in human lung tissue relative to that of other mucosal and non-

545   mucosal tissues (Fig 7). Our analysis suggests that human lung tissue could confer

546   heightened levels of pre-existing immune protection against multiple respiratory viruses

547   immediately upon pathogen entry. Importantly, this was not due to the elevated expression of

548   all ISGs, but rather tissue-specific profiles of individual ISG expression (Fig 7A-E, S2A

549   Table). These data demonstrate that human tissues confer distinct profiles of ISG expression

550   in a tissue-dependent manner which may confer enhanced protection at exposed surfaces.

551   While it remains to be determined how such distinct patterns of ISG expression occur, some

552   plausible explanations include: (i) the presence of commensal microbiota or natural turnover

553   of cells, stimulating low levels of PRR activation and IFN secretion through the release of

554   PAMPs or DAMPs, respectively [18, 83]; (ii) differential patterns of cytokine secretion

555   between tissues, including low basal levels of 'tonic' IFN signalling to maintain immune-

556   readiness and fitness [68, 69, 84, 85]; (iii) tissue-specific patterns of transcriptional regulation

557   occurring through cellular differentiation, which may be further influenced by inherited

558   genetic traits or epigenetic status [85-88]. Importantly, these explanations are not mutually

559   exclusive, which may account for the variance in individual ISG expression profiles observed

560   between human tissue samples (Fig 7B). Further work is required to determine how such

561   tissue-specific signatures of pre-existing antiviral gene expression influence the initiation and

562   outcome of respiratory virus infection.

563   In conclusion, we identify pre-existing tissue-specific and cell-type dependent

564 patterns of constitutive immune gene expression which confer a significant intracellular

565 immune barrier to IAV replication from the outset of infection and independently of

566 pathogen-induced cytokine-mediated innate immune defences. These intrinsic barrier

567 defences are downregulated in many transformed cell lines currently used for respiratory

568 virus research, which share common networks of immune system disruption relevant to the

569 immune regulation of many respiratory pathogens.

570

Materials and Methods

Antibodies

Polyclonal antibodies were used to detect TRIM22 (Sigma-Aldrich; HPA003575), Mx1 (Santa Cruz; sc-50509), GBP1 (Proteintech; 15303-1-AP), IFIH1 (Proteintech; 21775-1-AP), TLR3 (Proteintech; 17766-1-AP), histone H3K27ac (AbCam; ab4729), and actin (Sigma-Aldrich; A5060). IAV hybridoma antisera were used to detect NP, M1, and NS1, as previously described [89]. Monoclonal antibodies were used to detect UBA7 (AbCam; ab133499), Actin (DSHB; 224-236-1), IFITM1 (Proteinech; 60074-1g), and IAV NP (AbCam; ab20343). Secondary antibodies were Alexa 488 and 555 donkey anti-mouse and -rabbit (Invitrogen; A21202, A21206, and A31572), DyLight 680- or 800-conjugated anti-rabbit (Thermo Fisher Scientific; 35568 and SA5-35571), and peroxidase conjugated anti-mouse (Sigma-Aldrich; A4416).

Animals and ethics

No animals were directly subjected to experimentation as part of this scientific study. All animal tissues were obtained from material produced in previously described experiments [65] with permission from Public Health England (PHE). Procedures associated with this earlier study were approved by the PHE Ethical Review Committee (Porton Down, UK) and authorized under UK Home Office project licence 30/3083.

Quantitative Histopathology of cynomolgus macaque tissue sections

Formalin fixed and paraffin embedded tissue samples were processed for haematoxylin and TRIM22 immunohistochemistry (IHC) staining, as previously described [65]. Tissue sections were independently assessed for TRIM22 expression by a qualified pathologist. Automated quantitation of TRIM22 expression levels in stained tissue sections was performed using whole-slide scans and Image-Pro Premier (Media Cybernetics), as previously described [90, 91].

Quantitative Histopathology of human tissue sections

IHC data from human tissue samples was obtained from the Human Protein Atlas (HPA; http://www.proteinatlas.org; [62, 63]) under a Creative Commons Attribution-ShareAlike 3.0 International License. The original images consulted were TRIM22 Bronchus (http://www.proteinatlas.org/ENSG00000132274-TRIM22/tissue/bronchus#img) and TRIM22 Nasopharynx (http://www.proteinatlas.org/ENSG00000132274-TRIM22/tissue/nasopharynx#img).

RNA-seq analysis of human cell lines and tissues

RNA-seq data for human cell lines (HBEC3-KT, A549, HEK 293, and HeLa) and human tissue biopsies (as indicated) were obtained from Human Protein Atlas (HPA; http://www.proteinatlas.org, version 18.1; [62, 63]) under a Creative Commons Attribution-ShareAlike 3.0 International License or Genotype-Tissue Expression (GTEx; https://gtexportal.org/home/, V7; [64]) project (as stated) supported by the Common Fund of the Office of Director of the National Institutes of Health, and by NCI, NHGRI, NHLBI, NIDA, NIMH, and NINDS. Principle Component Analysis (PCA) cluster plots were generated using kmeans and clusplot packages and prcomp function in R (https://www.r-project.org). Heatmaps were generated using Prism 8 (GraphPad) or pheatmap (v1.0.12) and cluster (v2.0.7-1) package in R. Network analysis was conducted using STRING (https://string-db.org; [72]).

Cells, viruses, and drugs

Primary human foetal lung fibroblast (MRC5) cells were purchased from the European Collection of Authenticated Cell Cultures (ECACC; 05072101). MRC5t cells are immortalized MRC5 cells expressing the catalytic subunit of human telomerase (hTERT), and were generated as previously described [92]. MRC5 and MRC5t cells were cultured in Dulbecco's Modified Eagle Medium (DMEM; Life Technologies; 41966) supplemented with

621   10 % foetal bovine serum (FBS; Life Technologies; 10270), 100 U/ml of penicillin and 100

622   µg/ml of streptomycin (P/S; Life Technologies; 15140-122), and 1× non-essential amino

623   acids (NEAA; Life Technologies 11140-035). MRC5t cells were supplemented with 5 µg/mL

624   hygromycin B (Thermo Fisher Scientific; 10687010) to maintain hTERT expression. MRC5t

625   cells were transduced with lentiviruses to express short hairpin (sh) RNAs based on the 19-

626   mer sequences; non-targeting control (shCtrl; 5'-TTATCGCGCATATCACGCG-3') or

627   TRIM22 targeting (shTRIM22 clone B7 [3' UTR]; 5'-TATTGGTGTTCAAGACTAT-3',

628   clone B8; 5'-CTGTACGCACCTGCACATT-3', clone B9; 5'-

629   GTGTCTTCGGCTGCCAATA-3'), as previously described [46]. Pooled, stably transduced

630   cells were maintained in growth media supplemented with 0.5 µg/ml puromycin (Sigma-

631   Aldrich; P8833). Primary human bronchial epithelial (HBEp) cells were purchased from

632   Sigma-Aldrich (502-05a). hTERT and CDK4 immortalized human bronchial epithelial cells

633   (HBEC3-KT) were purchased the Hamon Center for Therapeutic Oncology Research (UT

634   Southwestern Medical Center; [93]). Cells were cultured according to supplier guidelines.

635   Madin Darby Canine Kidney (MDCK; a gift from Ben Hale University of Zurich), human

636   lung adenocarcinoma epithelial (A549; PHE Culture Collections, 86012804), human

637   embryonic kidney (HEK 293T; a gift from Roger Everett MRC-UoG CVR) and human

638   cervical carcinoma (HeLa [a gift from Juergen Hass University of Edinburgh] or HEp2 [a gift

639   from Roger Everett MRC-UoG CVR]) cells were cultured in DMEM with 10 % FBS and

640   P/S. All cells were maintained at 37°C in 5 % CO_2. IAV strains A/WSN/1933(H1N1)

641   (WSN), A/Puerto Rico/8/1934(H1N1) (PR8), A/Udorn/307/1972(H3N2) (Udorn), and

642   A/California/04/2009(H1N1) (Cal) were propagated in MDCK cells.

643   A/Duck/Singapore/5/1997(H5N3) (Duck H5N3) and A/Chicken/Italy/1067/1999(H7N1)

644   (Chicken H7N1) were propagated in embryonated chicken eggs. WSN titres were calculated

645   by immunocytochemistry (ICC) plaque assay, as described below. PR8, Udorn, Duck H5H3

646   and Chicken H7N1 titres were calculated based on fluorescence forming units (FFU),

647   calculated from the proportion of NP-positive MRC5t cells detected at 8 hours post-infection

648   (hpi) by immunofluorescence confocal microscopy. Cells were interferon stimulated by the

649   addition of 100 IU/ml recombinant interferon-β (IFN-β; Merck, 407318) to the growth media

650   for 24 h. Cycloheximide (CHX; Sigma-Aldrich, C-7698) was prepared in Milli-Q water and

651   used at 10 μg/ml. Ruxolitinib (Ruxo; Selleckchem; S1378) was prepared in DMSO and used

652   at the concentrations indicated.

653   **Plaque and virus yield assays**

654   For plaque assays, cells were seeded at 2×10^5 cells/well in 12-well dishes and incubated for

655   a minimum of 16 h prior to manipulation. Cells were infected with serial dilutions of virus for

656   1 h at 37°C prior to overlay with conditioned growth medium supplemented with 1.2 %

657   Avicel (Biopolymers; RC-591), 0.1 % sodium bicarbonate (Life Technologies; 25080-060),

658   and 0.01 % DEAE Dextran (Sigma-Aldrich; D9885). Cell monolayers were processed for

659   ICC staining at 24 to 72 hpi depending on virus replication kinetics (as previously described

660   [94]) or stained with Giemsa stain (VWR; 35086). Relative plaque titre was calculated as the

661   plaque titre of a virus stock under the indicated condition divided by its titre under a control

662   condition. For virus yield assays, cells were infected with IAV (WSN) at the indicated

663   multiplicity of infection (MOI) for 1 h at 37°C, washed twice with PBS, then overlaid with

664   growth medium. Supernatants were collected at the indicated time points post-infection and

665   the released virus was titred by plaque assay in MDCK cells. Plaque diameters were

666   measured using an automated Celigo imaging cytometer (Nexcelom biosciences), as per the

667   manufacturer's instructions.

668   **Immunofluorescence confocal microscopy**

669   1×10^5 cells were seeded on 13 mm glass coverslips in 24-well dishes and incubated for a

670   minimum of 16 h prior to manipulation. After treatment, cell monolayers were fixed,

671 permeabilized, and immunostained at the indicated time points, as previously described [94].

672 Nuclei were stained with DAPI (Sigma-Aldrich, D9542). Coverslips were mounted on glass

673 slides using Citiflour AF1 mounting medium (AgarScientific; R1320) and sealed with nail

674 enamel. Samples were examined with a Zeiss LSM 880 or LSM 710 confocal microscope

675 with 405, 488, 543, and 633-nm laser lines. Images were captured under a Plan-Apochromat

676 63×/1.4 oil immersion or Plan-Neofluar 20×/0.5 air objective lenses. The proportion of IAV

677 NP antigen positive cells was calculated from a minimum of five wide field images, imaging

678 more than 1000 cells per coverslip per condition. The proportion of NP positive cells was

679 determined and the fold increase in NP positive cells between IAV infected shTRIM22 and

680 shCtrl MRC5t cells calculated for each biological repeat.

681 **Western Blotting**

682 Cells were seeded at 2×10^5 cells/well in 12-well dishes and incubated for a minimum of 16

683 h prior to manipulation. Treated or infected cell monolayers were washed twice in PBS and

684 whole cell lysates (WCLs) collected in Laemmli buffer. Proteins were resolved on NOVEX

685 NU-PAGE (4-12%) Bis-Tris gels (Invitrogen; NP0322), transferred onto 0.22 μm

686 nitrocellulose membranes (Amersham; 15249794), and probed by western blotting, as

687 previously described [94]. Membranes were imaged using an Odyssey Infrared Imager (Li-

688 Cor). Band intensities were quantified using Image Studio Software (Li-Cor).

689 **qRT-PCR**

690 For viral or cellular mRNA quantitation, cells were seeded at 2×10^5 cells/well in 12-well

691 dishes and incubated for a minimum of 16 h prior to manipulation. Treated or infected cell

692 monolayers were washed once in PBS prior to RNA extraction using an RNAeasy Plus Kit

693 (Qiagen; 74134). mRNA was reverse transcribed (RT) using the TaqMan Reverse

694 Transcription Reagents kit (Life Technologies; N8080234) with oligo (dT) primers. Samples

695 were analysed in triplicate using the TaqMan Fast Universal PCR Master Mix (Life

696   Technologies, 4352042) and TaqMan *GAPDH* (4333764F), *TRIM22* (Hs01001179_m1), *Mx1*

697   (Hs00895608_m1) or *ISG15* (Hs01921425_s1) specific primer-probe (FAM/MGB; Thermo

698   Fisher Scientific) mixes or custom IAV (*NP*, *M1*, *NS1*/*NEP*) primer-probes mixes (S7 Table).

699   The ΔΔCt method was used to normalize transcript levels to those of *GAPDH* mRNA. For

700   vRNA analysis, cells were seeded at 4×10^5 cells/well in 6-well plates and incubated for a

701   minimum of 16 h prior to manipulation. Cells were infected either in the presence or absence

702   of CHX. At the indicated time points, cell monolayers were washed in PBS, harvested by

703   trypsinization, and cell pellets washed twice in ice cold PBS. Nuclear and cytoplasmic

704   fractions were isolated using NucBuster (Novagen 71183-3). If appropriate, fractions were

705   divided for both western blot and qRT-PCR analysis. For vRNA analysis, total RNA was

706   isolated from nuclear pellets using an RNAeasy Plus Kit. An IAV segment 7 specific primer

707   (5'-AGCCGAGATCGCACAGAGACTT-3') was used for reverse transcription, as

708   previously described [95]. Samples were analysed in triplicate using the M1 primer-probe

709   mix relative to a synthetic segment 7 (M) vRNA reference standard. The segment 7 vRNA

710   standard was produced as previously described [95]. Briefly, vRNA was extracted from

711   infected MDCK cells using the QIAamp Viral RNA Mini kit (Qiagen, 52904) and extracted

712   RNA was reverse transcribed using the Uni12 universal IAV segment primer (5'-

713   AGCAAAAGCAGG-3') and TaqMan Reverse Transcription Reagent kit. The cDNA was

714   used as a template to amplify the IAV segment 7 ORF, incorporating a T7 promoter sequence

715   that was used to generate synthetic segment 7 vRNA using the TranscriptAID T7 high yield

716   transcription kit (Thermo Fisher Scientific; K0441). Synthetic vRNA was purified using an

717   RNAeasy column and used as a reference standard for reverse transcription and qRT-PCR

718   analysis.

Plasmids and transfections

A cDNA encoding wild-type (WT) human TRIM22 (a gift form Professor Juergen Hass,

University of Edinburgh) was inserted into pcDNA.3.1 (Invitrogen) in frame with a 5' Myc-

tag oligo to generate a pcDNA.Myc.TRIM22. Clones were verified by Sanger sequencing.

The IAV (WSN) pcDNA-NP (WSN) expression plasmid has been described previously [96,

97]. All transfections were performed using Lipofectamine 2000 (Thermo Fisher Scientific;

11668). For NP stability assays, 1 x 10^5 HEK 293T cells/well were seeded onto poly-lysine

(Sigma; 7405) coated 24-well plates. 24 h post-seeding, cells were co-transfected with 150 ng

of pcDNA-NP (WSN) and 0, 100, 200, or 250 ng of pcDNA.Myc.TRIM22. Input levels of

DNA were equalized by the inclusion of pcDNA.3.1 empty vector. Cells were harvested 24 h

post-transfection and WCLs analysed by western blotting.

Figure Legends

FIG 1. TRIM22 is constitutively expressed in the respiratory tract independently of IAV

infection. (A) mRNA transcript levels (log2 transcripts per million; TPM) of TRIM family

members in human lung tissue (S1A Table). Black line: median TRIM transcript expression;

whisker: 5th to 95th percentile range. (B) TRIM22, TRIM32, and TRIM41 transcript levels

across a range of human tissues (S1B Table). Black line: median; whisker: 5th to 95th

percentile range. (C) Histological sections of human respiratory epithelium from the upper

(nasopharynx; patient ID 3624) and lower (bronchus; patient ID 3987) airway. TRIM22 is

labelled by immunohistochemistry (IHC; brown) and tissue counterstained with

haematoxylin and eosin. Scale bars are 50 μm. (D) Quantitation of TRIM IHC staining across

a range of tissue (as indicated). Red bars: Quantitation of TRIM22 in lung tissue sections. (A-

D) Data adapted under creative commons license from the Human Protein Atlas (HPA;

https://www.proteinatlas.org; [62, 63]). (E) Confocal micrographs of primary human

bronchial epithelial (HBEp) cells stained for TRIM22 by indirect immunofluorescence

(green). Nuclei stained with DAPI (blue). Scale bars; 10 μm (top panel) and 20 μm (bottom

panel). (F-H) Primary HBEp cells were treated with (+) or without (-) IFN-β (100 IU/ml) for

24 h. (F) Western blots of HBEp whole cell lysates (WCLs) probed for TRIM22 and Mx1

expression. Actin is shown as a loading control. (G) Quantitation of western blots (as shown

in F). Values normalized to actin and expressed relative to no IFN treatment; n=3, means and

standard deviation (SD) shown. (H) qRT-PCR for *TRIM22* and *Mx1* mRNA transcript levels

in control or IFN treated HBEp cells. Values normalized to no IFN treatment; n=3, means

and SD shown. (I) Histological sections of uninfected or influenza A virus (IAV;

A/California/04/09(H1N1), Cal) infected cynomolgus macaque respiratory epithelium from

the bronchus and alveoli (as indicated). TRIM22 is labelled by IHC (brown) and tissue

counterstained with haematoxylin. Scale bars; 50 and 20 μm (left and right panels,

760   respectively). (J) Automated quantitation of TRIM22 IHC staining in uninfected or infected

761   cynomolgus macaque respiratory tissue from whole-slide scans. Means and SD from four

762   uninfected and three infected animals are shown.

763

764   **FIG 2. TRIM22 is constitutively expressed in human diploid lung cells.** (A-C) Primary

765   and hTERT immortalized human lung fibroblast (MRC5 and MRC5t, respectively), human

766   lung adenocarcinoma epithelial (A549), and SV40-transformed human kidney epithelial

767   (HEK 293T; 293T) cells were treated with (+) or without (-) IFN-β (100 IU/ml) for 24 h. (A)

768   Western blots of WCLs probed for TRIM22 expression. Actin is shown as a loading control.

769   (B/C) qRT-PCR quantitation of *TRIM22* and *Mx1* mRNA transcript expression levels,

770   respectively. Values normalized to MRC5t cells without IFN treatment; n=3, means and SD

771   shown. (D) Confocal micrographs of MRC5t and A549 cells with or without IFN treatment

772   (as described in A). TRIM22 labelled by indirect immunofluorescence. Nuclei stained with

773   DAPI. (E) MDCK, 293T, A549, and MRC5t cells were infection with IAV (A/Puerto

774   Rico/8/1934(H1N1), PR8) at a MOI of 1 PFU/cell (based on MDCK cell titres) in the

775   presence of cycloheximide at 2 h prior to nuclear extraction and RNA isolation. qRT-PCR

776   quantitation of PR8 segment 7 (seg. 7) viral RNA (vRNA) levels in isolated nuclei. Black

777   circles: synthetic seg. 7 vRNA loading control standards (ng); Black line: semilog non-linear

778   regression ($R^2 = 0.99$); Red squares: seg. 7 vRNA levels detected in the nuclei of infected

779   cells (as indicated). (F) Seg. 7 vRNA levels (as shown in E) expressed relative to vRNA

780   levels isolated from infected MDCK nuclei. (E/F) n=3, means and SD shown. (G) Cell

781   monolayers were infected with serial dilutions of IAV (A/WSN/1933(H1N1), WSN). Plaque

782   numbers in each cell line were expressed relative (rel.) to MDCK cells (rel. plaque titre); n=3,

783   means and SD shown. One-way ANOVA Kruskal-Wallis test (*** $P < 0.001$; ns, not

784   significant).

785

786 **FIG 3. Constitutive TRIM22 expression confers intrinsic antiviral immunity.** (A)

787 MRC5t and A549 cells were mock-treated, IFN- β (100 IU/ml) stimulated or infected with

788 IAV (A/WSN/1933(H1N1), WSN) at a MOI of 1 PFU/cell (based on MDCK titres) for the

789 indicated times (h). Western blots of infected or treated WCLs (as indicated) probed for

790 TRIM22, Mx1, and viral protein (NP and NS1) expression. Actin is shown as a loading

791 control. (B) A549 cells were infected with IAV (WSN; MOI of 0.01 PFU/cell based on

792 MDCK titres) and harvested at the indicated times prior to western blotting (as in A). (C-E)

793 MRC5t and A549 cells were stably transduced to express non-targeting control (shCtrl) or

794 TRIM22-targeting (shTRIM22) shRNAs. (C) qRT-PCR quantitation of *TRIM22* mRNA

795 levels in MRC5t shCtrl and shTRIM22 cells. Values normalized to shCtrl; n=3, means and

796 SD shown. (D) MRC5t shCtrl and shTRIM22 cells were treated with (+) or without (-) IFN-β

797 (100 IU/ml) for 24 h. WCLs were analysed by western blotting for TRIM22 and Mx1. Actin

798 is shown as a loading control. (E) Western blot analysis of A549 shCtrl and shTRIM22

799 treated cells (as in D). (F) MRC5t and A549 shCtrl and shTRIM22 cells were infected with

800 IAV (WSN) at 0.001 PFU/cell (based on parental cell line titres). Media were harvested at the

801 indicated time points and IAV plaque titres determined on MDCK cells; n=3, means and SD

802 shown. (G) Representative immunocytochemistry images of IAV plaque formation (NP

803 staining) in MRC5t and A549 infected shCtrl and shTRIM22 cell monolayers (50-100

804 PFU/monolayer based on parental cell line titres). (H) Relative (rel.) IAV plaque titre (plaque

805 titre in shTRIM22 cells / plaque titre in shCtrl cells) in MRC5t and A549 infected cell

806 monolayers. All data points shown; line: mean. One-sample two-tailed t test (hypothetical

807 mean of 1; ** $P < 0.005$; ns, not significant).

808

809   **FIG 4. Constitutive TRIM22 expression restricts IAV infection independently of the**

810   **induction of cytokine-mediated innate immune defences.** (A) MRC5t cells were pre-

811   treated for 1 h with increasing concentrations (μM) of Ruxolitinib (Ruxo) or DMSO (carrier

812   control) prior to stimulation with (+) or without (-) IFN-β (100 IU/ml) for 24 h (in the

813   presence or absence of drug, as indicated). qRT-PCR quantitation of ISG (*Mx1* and *ISG15*)

814   mRNA levels from RNA extracted from treated cells. Values normalized to DMSO-only

815   treatment; RQ and RQmin/max plotted. (B) Quantitation of relative (rel.) IAV (WSN) plaque

816   titre (# plaques shTRIM22/# plaques shCtrl) in MRC5t cell monolayers treated with Ruxo (4

817   μM) or DMSO (as in A). Values normalized to infected shCtrl cell monolayers treated with

818   DMSO per experiment. All data points shown; line: mean. One-sample two-tailed t test

819   (hypothetical mean of 1; ** $P < 0.005$; ns, not significant).

820

821   **FIG 5. Constitutive TRIM22 expression restricts the initiation of IAV infection in a**

822   **strain independent manner.** MRC5t shCtrl or shTRIM22 cells were individually infected

823   with a panel of human (WSN, PR8, and A/Udorn/307/1972(H3N2); Udorn) or avian

824   (A/Duck/Singapore/5/1997(H5N3); Duck and A/Chicken/Italy/1067/1999(H7N1); Chicken)

825   IAVs at a MOI of 0.05 FFU/cell (based on MRC5t titres) for 8h. (A) Representative confocal

826   micrographs of PR8 infected MRC5t shCtrl or shTRIM22 cells. TRIM22 and IAV NP

827   labelled by indirect immunofluorescence. Nuclei stained with DAPI. (B) Relative (Rel.) fold

828   increase in NP antigen positive cells (shTRIM22/shCtrl) in IAV infected MRC5t cell

829   monolayers. n ≥ 3, all data points shown; line: mean.

830

831   **FIG 6. Constitutive TRIM22 expression restricts IAV transcription.** (A-B) MRC5t shCtrl

832   and shTRIM22 cells were infected with IAV (PR8) at a MOI of 0.05 PFU/cell (based on

833   MDCK titres) in the presence of cycloheximide for 4 h prior to nuclear (nuc.) or cytosolic

834   (cyto.) fractionation. (A) Western blot analysis showing histone H3 (nuc.) and actin (cyto.)

835   expression profiles in fractionated lysates. (B) qRT-PCR quantitation of IAV PR8 seg. 7

836   vRNA levels in nuclear fraction lysates. Values normalized to shCtrl per experiment (dotted

837   line). All data points shown; line: mean. One-sample two-tailed t test (hypothetical mean of

838   1; ns, not significant). (C, D) HEK 293T cells were transfected with increasing amounts of

839   myc-tagged TRIM22 expression plasmid, 150 ng of NP (WSN) expression plasmid, and

840   varying concentrations of empty vector control to balance DNA content for 24 h. (C) Western

841   blot analysis of WCLs showing TRIM22 and NP expression levels. Actin is shown as a

842   loading control. (D) Quantitation of NP expression protein levels (as in C). Values

843   normalized to actin and expressed relative to NP in the absence of TRIM22. n=3, means and

844   SD shown. (E-H) MRC5t shCtrl and shTRIM22 cells were infected with IAV (PR8) at a MOI

845   of 0.05 (E) or 0.2 (F-H) PFU/cell (based on MRC5t titres) and harvested at the indicated time

846   points. (E) Quantification of IAV vRNA seg. 7 levels by qRT-PCR. Values normalized to

847   infected shCtrl samples at 0.25 hpi. n=3, means and SD shown. (F) qRT-PCR quantitation of

848   IAV *NP*, *M1*, and *NS1/NEP* mRNA levels. Values normalized to infected shCtrl samples at 4

849   hpi. n=3, means and SD shown. (G) Western blots of infected WCLs showing viral (NP, M1,

850   and NS1) protein expression levels. Actin is shown as a loading control. (H) Quantitation of

851   viral protein expression levels (as in G). Values normalized to actin and expressed relative to

852   levels in infected shCtrl cells at 10 hpi. n=3, means and SD shown.

853

854   **FIG 7. Lung tissue is enriched for constitutive ISG expression.** (A) log2 median TPM

855   expression values of 200 ISGs [67] across a range of human tissue biopsies (n); lung (n=427),

856   small intestine (Int.; terminal ileum; n=137), esophagus (Espho.; mucosa; n=407), colon

857   (sigmoid; n=233), liver (n=175), skin (suprapubic; n=387), and kidney (cortex; n=45). Every

858   second gene labelled (full gene list in S2A Table). (B) Violin plots showing individual ISG

859   expression profiles of the top 50 constitutively expressed lung ISGs and associated

860   expression profiles in small intestine, skin, and kidney tissues. White line; median. Box; 5th

861   and 95th percentile range. (C) Violin plot showing tissue expression profile of 200 ISGs

862   across human tissues (as in A). Horizontal solid lines; median ISG expression per tissue.

863   Horizontal dotted lines; 5th and 95th percentile range per tissue. (D) Principle component (PC)

864   plot showing clustered ISG expression profiles across all tissues. (E) Heatmap showing

865   clustered ISG transcript expression profiles between tissues. (F) log2 median TPM tissue

866   expression values of IFN-related receptors and cytokines across human tissues (as in A; S2B

867   Table). (G) Violin plot showing the median tissue expression values of IFN-related receptors

868   and cytokines across human tissues (as in F). Horizontal solid lines; median. Horizontal

869   dotted lines; 5th and 95th percentile range. Paired one-way ANOVA (Friedman multiple

870   comparison test); **** $P < 0.0001$; ns, not significant. RNA-seq data adapted under creative

871   commons licence from GTEx portal (https://gtexportal.org/home/; [64]).

872

873   **FIG 8. Virally-transformed cells have downregulated levels of constitutive ISG**

874   **expression.** (A) log2 TPM expression values of constitutive expressed ISGs ($\geq$ 5 TPM per

875   gene; 87 of 178 genes, S3A Table) in non-treated HBEC3, A549, HEK 293 (293), and HeLa

876   cells. (B) Differentially downregulated ISGs (HBEC3 $\geq$ 5-fold change; as in A) plotted

877   against the equivalent log2 median TPM ISG tissue expression values obtained from human

878   lung tissue biopsies (n=427) (S3B Table). Downregulated ISGs common to three transformed

879   cell lines; core: common to two transformed cell lines; shared: unique to one transformed cell

880   line; unique. (D/E) High-confidence (> 0.7) STRING (https://string-db.org; [72]) protein-

881   protein interaction (PPI) network of identified downregulated ISGs (as in B). Core; blue

882   circles: shared; purple circles: unique; grey circles. Network PPI enrichment: $P < 1.0e-16$.

883   Ranked biological process (GO), KEGG pathways (green circles in D), and reference

884   publications (red and blue circles in D; [70, 71]) with associated counts in gene sets (count)

885   and FDR (false discovery rate) values shown. Cell line and tissue RNA-seq data adapted

886   under creative commons licence from HPA and GTEx portal, respectively [62-64].

887

888   **FIG 9. Transformed cells are deficient in the constitutive expression of multiple immune**

889   **regulators.** (A) Scatter plots highlighting downregulated genes (blue circles) identified

890   between non-treated HBEC3 cells ($\geq$ 3 TPM; median HBEC3 TPM per gene, horizontal

891   dotted line) and A549 (median 3 TPM per gene), HEK 293 (293; median 3 TPM per gene), or

892   HeLa cells (median 4 TPM per gene; $\leq$ 4 TPM, vertical dotted line; HBEC3 $\geq$ 5-fold change,

893   diagonal dotted line; S4A Table). Differentially downregulated genes were mapped and used

894   for pathway analysis using Reactome (https://reactome.org; Table S4B). The number of

895   downregulated genes and percentage mapped to the immune system (% immune-related;

896   Table S4C) is shown. (B) log2 TPM gene expression profiles of downregulated immune

897   system genes (as in A; 174 unique genes identified, every second labelled). Downregulated

898   genes common to three transformed cell lines; core: common to two transformed cell lines;

899   shared: unique to one transformed cell line; unique (as highlighted; S4D Table). (C) High-

900   confidence (> 0.7) STRING protein-protein interaction (PPI) network of identified

901   downregulated immune system genes (as in B). Core; blue circles: shared; purple circles:

902   unique; grey circles. Network PPI enrichment: P < 1.0e-16. Ranked biological process (GO)

903   and KEGG pathways with associated counts in gene sets (count) and FDR (false discovery

904   rate) values shown. An enlarged annotated map is presented in S5 Fig. Cell line RNA-seq

905   data adapted under creative commons licence from HPA [62, 63].

906

907   **FIG 10. Transformed cells are permissive to IAV replication independently of**

908   **pathogen-induced cytokine-mediated innate immune defences.** (A) log2 TPM expression

909   values of 184 IAV immuno-regulatory genes (extended IAV KEGG network (hsa05164);

910   [70]; S5A Table) in non-treated HBEC3, A549, HEK 293 (293), and HeLa cells. Every

911   second gene labelled. (B) Differentially downregulated IAV immuno-regulatory IAV genes

912   (HBEC3 $\geq$ 5-fold change, $\geq$ 3 TPM per gene) plotted against the equivalent log2 median

913   TPM gene expression values obtained from human lung tissue biopsies (n=427) (S5B Table).

914   (A, B) Cell line and tissue RNA-seq data adapted under creative commons licence from HPA

915   and GTEx portal, respectively [62-64]. (C) Violin plot showing log2 TPM expression values

916   of downregulated IAV immuno-regulatory genes (as in B). Horizontal solid lines; median

917   gene expression. Horizontal dotted lines; 5th and 95th percentile range. Paired one-way

918   ANOVA (Friedman multiple comparison test); ** $P < 0.01$; **** $P < 0.0001$; ns, not

919   significant. (D) High-confidence (> 0.7) STRING protein-protein interaction (PPI) network

920   of identified downregulated KEGG associated IAV genes (as in B). Core; blue circles:

921   shared; purple circles: unique; grey circles. Network PPI enrichment: $P < 1.0e-16$. (E)

922   Western blots of non-treated HBEC3 and A549 WCLs showing UBA7, GBP1, IFIH1, TLR3,

923   IFITM1, and TRIM22 (+ve control) protein expression levels. Actin is shown as a loading

924   control. (F) Quantitation of protein expression levels (as in E). Values normalized to actin

925   and expressed relative to levels in HBEC3 cells. n$\geq$3, means and SD shown. One-sample

926   two-tailed t test (hypothetical mean of 1; ** $P < 0.005$, **** $P < 0.0001$). (G) Representative

927   immunocytochemistry images of IAV plaque formation (NP staining) in MDCK, A549, and

928   HBEC3 cells infected with equivalent serial dilutions of IAV (WSN). (H) Quantitation of

929   plaque numbers in each cell line expressed relative (rel.) to MDCK cells (rel. plaque titre);

930   n$\geq$3, means and SD shown. Mann-Whitney U-test; **** $P < 0.0001$. (I) MDCK, A549, and

931   HBEC3 cells were pre-treated for 1 h in the presence of Ruxolitinib (Ruxo; 5 μM) or DMSO

932   (carrier control) prior to infection with serial dilutions of IAV (WSN; in the presence of drug

933   or carrier control). Quantitation of rel. plaque titre (plaque titre with Ruxo / plaque titre with

934   DMSO) for each cell line is shown. n≥3, means and SD shown. One-sample two-tailed t test

935   (hypothetical mean of 1; ns, not significant). (J) Quantitation of the fold increase in IAV

936   plaque diameter in Ruxo or DMSO-treated infected cell monolayers (as in I). Values

937   normalized to the median DMSO plaque diameter in each cell line (DMSO or Ruxo/median

938   DMSO). n≥3, means and SD shown. Mann-Whitney U-test; **** $P < 0.0001$.

939

Supplemental Figure Legends

941   **S1 FIG. TRIM22 is constitutively expressed to high level in lung tissue.** (A) Transcript

942   expression levels (log2 median TPM) of 67 TRIM family members in human lung tissue

943   biopsies (n=457; S1A Table). Black line: median TRIM transcript expression; whisker: 5th to

944   95th percentile range. (B) Transcript expression levels (log2 median TPM) of TRIM22 across

945   a range of human tissues (S1C Table). Lung and spleen tissues are highlighted (red and blue

946   circles, respectively). Black line: median; whisker: 5th to 95th percentile range. (C, D) Violin

947   plots showing individual TRIM family member (C, lung) or TRIM22 (D, all tissues)

948   expression profiles (log10 TPM), respectively. White line; median. Box; 5th and 95th

949   percentile range. (A-D) Data adapted under creative commons license from GTEx portal

950   [64].

951

952   **S2 FIG. TRIM22 antibody validation.** MRC5t cells were stably transduced to express non-

953   targeting control (shCtrl) or TRIM22-targeting (shTRIM22, clones B7-B9) shRNAs. (A)

954   qRT-PCR quantitation of *TRIM22* mRNA levels in MRC5t shCtrl and shTRIM22 cells.

955   Values normalized to shCtrl. Mean RQ and RQ min/max shown. (B) Western blot of WCLs

956   derived from MRC5t shCtrl and shTRIM22 (clone B7) cells showing TRIM22 (detected

957   using pAb HPA003575; Sigma-Aldrich) expression levels. Actin is shown as a loading

958   control. (C) Confocal micrographs showing the nuclear localization of TRIM22 in MRC5t

959   shCtrl or shTRIM22 (clone B7) cells. TRIM22 was detected by indirect immunofluorescence

960   (pAb HPA003575; Sigma-Aldrich). Nuclei were stained with DAPI.

961

962   **S3 FIG. Constitutive TRIM22 expression is lost in many transformed cell lines.** MRC5

963   (primary lung fibroblast), MRC5t (telomerase immortalized MRC5), A549, HEK 293T

964   (293T), HeLa, and HEp2 cells were treated for 24 h with (+) or without (-) IFN-β stimulation

965   (100 IU/ml). (A) qRT-PCR quantitation of *TRIM22* mRNA transcript levels across the panel

966   of cell lines. Values normalized to *TRIM22* levels in MRC5t cells without IFN-β stimulation.

967   n=3, means and SD shown. (B) Western blots showing TRIM22 expression levels in WCLs

968   derived from the panel cell lines. Actin is shown as a loading control.

969

970   **S4 FIG. Identification of tissue-specific and cell-type dependent patterns of constitutive**

971   **ISG expression.** (A) Transcript expression profiles (log2 TPM) of 178 ISGs in HBEC3,

972   A549, HEK 293 (293), and HeLa cells plotted against the equivalent gene set from human

973   lung tissue biopsies (n=427; log2 median TPM shown). Every second gene labelled (S3A

974   Table). (B) Violin plot showing cell line and lung tissue ISG expression profiles (as in A).

975   Horizontal solid lines; median ISG expression. Horizontal dotted lines; 5th and 95th percentile

976   range. Paired one-way ANOVA (Friedman multiple comparison test); **** $P < 0.0001$. (C)

977   Heatmap showing clustered distribution of ISG transcript levels between cell lines and

978   human lung tissue (as in B). Cell line and tissue RNA-seq data adapted under creative

979   commons licence from HPA and GTEx portal, respectively [62-64].

980

981   **S5 FIG. Annotated STRING network of downregulated immune system genes in**

982   **virally-transformed cells.** Annotated high-confidence (> 0.7) STRING network of identified

983   differential downregulated immune system genes in virally-transformed cells (as shown in

984 Fig 9C; S4D Table). Downregulated ISGs common to three transformed cell lines; core, blue

985 circles: common to two transformed cell lines; shared, purple circles: unique to one

986 transformed cell line; unique, grey circles. Network PPI enrichment: $P < 1.0e\text{-}16$. Ranked

987 biological process (GO) and KEGG pathways with associated counts in gene sets (count) and

988 FDR (false discovery rate) values shown.

989

990 **S6 FIG. TRIM family expression profile in human lung tissue and lung epithelial**

991 **(HBEC3 and A549) cells.** (A) Transcript expression profile of 67 TRIM family members

992 derived from human lung tissue, hTERT immortalized (HBEC3), or virally-transformed

993 (A549) human lung epithelial cells. Data adapted under creative commons license from

994 Human Protein Atlas (HPA; [62, 63]) and Genotype-Tissue Expression (GTEx; [64]) project.

995 (B) Scatter plots showing the differential transcript expression of individual TRIM family

996 members between lung tissue data sets (GTEx and HPA), lung tissue (GTEx) and either

997 HBEC3 or A549, or between HBEC3 and A549 (as indicated). Solid coloured lines; linear

998 regression. Solid black lines; 95% confidence interval. R-squared (R^2) values indicated.

999 Selected TRIMs are highlighted for reference.

1000

1001 **Supplemental Tables**

1002 **S1 Tables. TRIM family member transcript expression values across a range of human**

1003 **tissues.** (S1A) HPA and GTEx transcript expression values of 67 TRIM family member

1004 genes in human lung tissue. (S1B) HPA transcript expression values of TRIM22, TRIM32,

1005 and TRIM41 across a range of human tissues (as indicated). (S1C) GTEx TRIM22 transcript

1006 expression values across a range of human tissues (as indicated). Data adapted under creative

1007 commons license from Human Protein Atlas (HPA; [62, 63]) and Genotype-Tissue

1008 Expression (GTEx; [64]) project.

1009

1010 **S2 Tables. ISG transcript expression values across a range of human tissues.** (S2A)

1011 Transcript expression values for 200 ISGs (previously shown to be upregulated $\geq$ 8-fold

1012 change in response to universal IFN treatment in primary cell culture; [67]) across a range of

1013 mucosal (lung, small intestine [int.; terminal ileum], esophagus [mucosa], colon [sigmoid]),

1014 and non-mucosal (liver, skin [suprapubic], and kidney [cortex] tissues. (S2B) Transcript

1015 expression values of IFN-related receptors and cytokines across human tissues (as in S2A).

1016 Data adapted under creative commons license from Genotype-Tissue Expression (GTEx;

1017 [64]) project.

1018

1019 **S3 Tables. Constitutive ISG transcript expression values across a range of cell lines and**

1020 **lung tissue.** (S3A) Transcript expression values for 178 ISGs (previously shown to be

1021 upregulated $\geq$ 8-fold change in response to universal IFN treatment in primary cell culture;

1022 [67]) across a range of non-treated transformed (A549, HEK 293, and HeLa) cells, hTERT

1023 immortalized (HBEC3) cells, or lung tissue. (S3B) ISG expression values of differentially

1024 downregulated ISGs between cell lines (HBEC3 $\geq$ 5-fold change, $\geq$ 5 TPM) and equivalent

1025 gene set tissue expression values obtained from human lung tissue biopsies (n=427, log2

1026 median TPM). Data adapted under creative commons license from Human Protein Atlas

1027 (HPA; [62, 63]) and Genotype-Tissue Expression (GTEx; [64]) project.

1028

1029 **S4 Tables. Constitutive immune system transcript expression values across a range of**

1030 **cell lines.** (S4A) Transcript expression values for differentially downregulated genes

1031 identified between non-treated HBEC3 ($\geq$ 3 TPM [median TPM all genes]) and A549

1032 [median 3 TPM all genes], HEK 293 [median 3 TPM all genes], or HeLa [median 4 TPM all

1033 genes] cells ($\leq$ 4 TPM; HBEC3 $\geq$ 5-fold change; blue circles in Fig 9A). (S4B) Reactome

1034   (https://reactome.org) pathway analysis of downregulated mapped genes (as in S4A; blue

1035   circles in Fig 9A). Red text highlights pathways relating to the immune system. (S4C)

1036   Uniprot IDs for downregulated genes mapped to the immune system (as in B; Reactome

1037   immune system). (S4D) Ranked transcript expression values for downregulated immune

1038   system genes identified in all three (core; blue), common to two (shared; purple), or unique to

1039   one (unique) transformed cell line(s). Data adapted under creative commons license from

1040   Human Protein Atlas (HPA; [62, 63]).

1041

1042   **S5 Tables. Extended IAV KEGG network transcript expression values across a range of**

1043   **cell lines and lung tissue.** (S5A) Transcript expression values of 184 IAV immuno-

1044   regulatory genes (extended (ext.) IAV KEGG network (hsa05164), [70]) in non-treated

1045   HBEC3, A549, HEK 293, and HeLa cells. (S5B) Transcript expression values of

1046   differentially downregulated IAV immuno-regulatory genes (HBEC3 $\geq$ 5-fold change, $\geq$ 3

1047   TPM) and equivalent gene set expression values obtained from human lung tissue biopsies

1048   (n=427; log2 median TPM). Data adapted under creative commons license from Human

1049   Protein Atlas (HPA; [62, 63]) and Genotype-Tissue Expression (GTEx; [64]) project.

1050

1051   **S6 Table. TRIM family member transcript expression values across a range of cell lines**

1052   **and lung tissue.** Transcript expression values of 67 TRIM family member genes across a

1053   range of non-treated cells (HBEC3, A549, HEK 293, and HeLa) and human lung tissue

1054   biopsies (n=427; log2 median TPM). Data adapted under creative commons license from

1055   Human Protein Atlas (HPA; [62, 63]) and Genotype-Tissue Expression (GTEx; [64]) project.

1056

1057   **S7 Table. Custom IAV primer-probe sequences.** Nucleotide sequences for custom IAV

1058   (*NP*, *M1*, *NS1*/*NEP*) primer-probes mixes used in the study.

References

1060   1.   Killip MJ, Fodor E, Randall RE. Influenza virus activation of the interferon system.
1061   Virus Res. 2015;209:11-22. Epub 2015/02/14. doi: 10.1016/j.virusres.2015.02.003. PubMed
1062   PMID: 25678267; PubMed Central PMCID: PMCPMC4638190.
1063   2.   Iwasaki A, Pillai PS. Innate immunity to influenza virus infection. Nat Rev Immunol.
1064   2014;14(5):315-28. Epub 2014/04/26. doi: 10.1038/nri3665. PubMed PMID: 24762827;
1065   PubMed Central PMCID: PMCPMC4104278.
1066   3.   Pulendran B, Maddur MS. Innate immune sensing and response to influenza. Curr
1067   Top Microbiol Immunol. 2015;386:23-71. Epub 2014/08/01. doi: 10.1007/82_2014_405.
1068   PubMed PMID: 25078919; PubMed Central PMCID: PMCPMC4346783.
1069   4.   Durbin RK, Kotenko SV, Durbin JE. Interferon induction and function at the mucosal
1070   surface. Immunol Rev. 2013;255(1):25-39. doi: 10.1111/imr.12101. PubMed PMID:
1071   23947345.
1072   5.   Schoggins JW, Wilson SJ, Panis M, Murphy MY, Jones CT, Bieniasz P, et al. A
1073   diverse range of gene products are effectors of the type I interferon antiviral response.
1074   Nature. 2011;472(7344):481-5. doi: 10.1038/nature09907. PubMed PMID: 21478870;
1075   PubMed Central PMCID: PMCPMC3409588.
1076   6.   Schoggins JW, MacDuff DA, Imanaka N, Gainey MD, Shrestha B, Eitson JL, et al.
1077   Pan-viral specificity of IFN-induced genes reveals new roles for cGAS in innate immunity.
1078   Nature. 2014;505(7485):691-5. Epub 2013/11/29. doi: 10.1038/nature12862. PubMed PMID:
1079   24284630; PubMed Central PMCID: PMCPMC4077721.
1080   7.   Tapia K, Kim WK, Sun Y, Mercado-Lopez X, Dunay E, Wise M, et al. Defective
1081   viral genomes arising in vivo provide critical danger signals for the triggering of lung
1082   antiviral immunity. PLoS Pathog. 2013;9(10):e1003703. Epub 2013/11/10. doi:
1083   10.1371/journal.ppat.1003703. PubMed PMID: 24204261; PubMed Central PMCID:
1084   PMCPMC3814336.
1085   8.   Killip MJ, Jackson D, Perez-Cidoncha M, Fodor E, Randall RE. Single-cell studies of
1086   IFN-beta promoter activation by wild-type and NS1-defective influenza A viruses. J Gen
1087   Virol. 2017;98(3):357-63. Epub 2016/12/17. doi: 10.1099/jgv.0.000687. PubMed PMID:
1088   27983470; PubMed Central PMCID: PMCPMC5721924.
1089   9.   Rodriguez A, Falcon A, Cuevas MT, Pozo F, Guerra S, Garcia-Barreno B, et al.
1090   Characterization in vitro and in vivo of a pandemic H1N1 influenza virus from a fatal case.
1091   PLoS One. 2013;8(1):e53515. Epub 2013/01/18. doi: 10.1371/journal.pone.0053515.
1092   PubMed PMID: 23326447; PubMed Central PMCID: PMCPMC3542358.
1093   10.   Vasilijevic J, Zamarreno N, Oliveros JC, Rodriguez-Frandsen A, Gomez G,
1094   Rodriguez G, et al. Reduced accumulation of defective viral genomes contributes to severe
1095   outcome in influenza virus infected patients. PLoS Pathog. 2017;13(10):e1006650. Epub
1096   2017/10/13. doi: 10.1371/journal.ppat.1006650. PubMed PMID: 29023600; PubMed Central
1097   PMCID: PMCPMC5638565.
1098   11.   Russell AB, Elshina E, Kowalsky JR, Te Velthuis AJW, Bloom JD. Single-cell virus
1099   sequencing of influenza infections that trigger innate immunity. J Virol. 2019. Epub
1100   2019/05/10. doi: 10.1128/JVI.00500-19. PubMed PMID: 31068418.
1101   12.   Kallfass C, Lienenklaus S, Weiss S, Staeheli P. Visualizing the beta interferon
1102   response in mice during infection with influenza A viruses expressing or lacking
1103   nonstructural protein 1. J Virol. 2013;87(12):6925-30. Epub 2013/04/12. doi:
1104   10.1128/JVI.00283-13. PubMed PMID: 23576514; PubMed Central PMCID:
1105   PMCPMC3676098.

1106   13.   Hale BG, Albrecht RA, Garcia-Sastre A. Innate immune evasion strategies of
1107   influenza viruses. Future Microbiol. 2010;5(1):23-41. doi: 10.2217/fmb.09.108. PubMed
1108   PMID: 20020828; PubMed Central PMCID: PMCPMC2820251.
1109   14.   Hsu AC. Influenza Virus: A Master Tactician in Innate Immune Evasion and Novel
1110   Therapeutic Interventions. Front Immunol. 2018;9:743. Epub 2018/05/15. doi:
1111   10.3389/fimmu.2018.00743. PubMed PMID: 29755452; PubMed Central PMCID:
1112   PMCPMC5932403.
1113   15.   Bieniasz PD. Intrinsic immunity: a front-line defense against viral attack. Nat
1114   Immunol. 2004;5(11):1109-15. doi: 10.1038/ni1125. PubMed PMID: 15496950.
1115   16.   Komatsu T, Nagata K, Wodrich H. The Role of Nuclear Antiviral Factors against
1116   Invading DNA Viruses: The Immediate Fate of Incoming Viral Genomes. Viruses.
1117   2016;8(10). doi: 10.3390/v8100290. PubMed PMID: 27782081; PubMed Central PMCID:
1118   PMCPMC5086622.
1119   17.   Everett RD, Boutell C, Hale BG. Interplay between viruses and host sumoylation
1120   pathways. Nat Rev Microbiol. 2013;11(6):400-11. Epub 2013/04/30. doi:
1121   10.1038/nrmicro3015. PubMed PMID: 23624814.
1122   18.   Liu BC, Sarhan J, Poltorak A. Host-Intrinsic Interferon Status in Infection and
1123   Immunity. Trends Mol Med. 2018;24(8):658-68. Epub 2018/08/01. doi:
1124   10.1016/j.molmed.2018.06.004. PubMed PMID: 30060835; PubMed Central PMCID:
1125   PMCPMC6084451.
1126   19.   Alandijany T, Roberts APE, Conn KL, Loney C, McFarlane S, Orr A, et al. Distinct
1127   temporal roles for the promyelocytic leukaemia (PML) protein in the sequential regulation of
1128   intracellular host immunity to HSV-1 infection. PLoS Pathog. 2018;14(1):e1006769. Epub
1129   2018/01/09. doi: 10.1371/journal.ppat.1006769. PubMed PMID: 29309427; PubMed Central
1130   PMCID: PMCPMC5757968.
1131   20.   Brass AL, Huang IC, Benita Y, John SP, Krishnan MN, Feeley EM, et al. The IFITM
1132   proteins mediate cellular resistance to influenza A H1N1 virus, West Nile virus, and dengue
1133   virus. Cell. 2009;139(7):1243-54. Epub 2010/01/13. doi: 10.1016/j.cell.2009.12.017. PubMed
1134   PMID: 20064371; PubMed Central PMCID: PMCPMC2824905.
1135   21.   Fu B, Wang L, Ding H, Schwamborn JC, Li S, Dorf ME. TRIM32 Senses and
1136   Restricts Influenza A Virus by Ubiquitination of PB1 Polymerase. PLoS Pathog.
1137   2015;11(6):e1004960. doi: 10.1371/journal.ppat.1004960. PubMed PMID: 26057645;
1138   PubMed Central PMCID: PMCPMC4461266.
1139   22.   Patil G, Zhao M, Song K, Hao W, Bouchereau D, Wang L, et al. TRIM41-Mediated
1140   Ubiquitination of Nucleoprotein Limits Influenza A Virus Infection. J Virol. 2018;92(16).
1141   doi: 10.1128/JVI.00905-18. PubMed PMID: 29899090.
1142   23.   Chen S, Short JA, Young DF, Killip MJ, Schneider M, Goodbourn S, et al.
1143   Heterocellular induction of interferon by negative-sense RNA viruses. Virology.
1144   2010;407(2):247-55. Epub 2010/09/14. doi: 10.1016/j.virol.2010.08.008. PubMed PMID:
1145   20833406; PubMed Central PMCID: PMCPMC2963793.
1146   24.   Russell AB, Trapnell C, Bloom JD. Extreme heterogeneity of influenza virus
1147   infection in single cells. Elife. 2018;7. Epub 2018/02/17. doi: 10.7554/eLife.32303. PubMed
1148   PMID: 29451492; PubMed Central PMCID: PMCPMC5826275.
1149   25.   Steuerman Y, Cohen M, Peshes-Yaloz N, Valadarsky L, Cohn O, David E, et al.
1150   Dissection of Influenza Infection In Vivo by Single-Cell RNA Sequencing. Cell Syst.
1151   2018;6(6):679-91 e4. Epub 2018/06/11. doi: 10.1016/j.cels.2018.05.008. PubMed PMID:
1152   29886109.
1153   26.   Frishberg A, Peshes-Yaloz N, Cohn O, Rosentul D, Steuerman Y, Valadarsky L, et al.
1154   Cell composition analysis of bulk genomics using single-cell data. Nat Methods. 2019. Epub
1155   2019/03/20. doi: 10.1038/s41592-019-0355-5. PubMed PMID: 30886410.

1156   27.   Ciancanelli MJ, Huang SX, Luthra P, Garner H, Itan Y, Volpi S, et al. Infectious
1157   disease. Life-threatening influenza and impaired interferon amplification in human IRF7
1158   deficiency. Science. 2015;348(6233):448-53. Epub 2015/03/31. doi:
1159   10.1126/science.aaa1578. PubMed PMID: 25814066; PubMed Central PMCID:
1160   PMCPMC4431581.
1161   28.   Ciancanelli MJ, Abel L, Zhang SY, Casanova JL. Host genetics of severe influenza:
1162   from mouse Mx1 to human IRF7. Curr Opin Immunol. 2016;38:109-20. Epub 2016/01/14.
1163   doi: 10.1016/j.coi.2015.12.002. PubMed PMID: 26761402; PubMed Central PMCID:
1164   PMCPMC4733643.
1165   29.   Mogensen TH. IRF and STAT Transcription Factors - From Basic Biology to Roles
1166   in Infection, Protective Immunity, and Primary Immunodeficiencies. Front Immunol.
1167   2018;9:3047. Epub 2019/01/24. doi: 10.3389/fimmu.2018.03047. PubMed PMID: 30671054;
1168   PubMed Central PMCID: PMCPMC6331453.
1169   30.   Honda K, Yanai H, Negishi H, Asagiri M, Sato M, Mizutani T, et al. IRF-7 is the
1170   master regulator of type-I interferon-dependent immune responses. Nature.
1171   2005;434(7034):772-7. Epub 2005/04/01. doi: 10.1038/nature03464. PubMed PMID:
1172   15800576.
1173   31.   Lazear HM, Lancaster A, Wilkins C, Suthar MS, Huang A, Vick SC, et al. IRF-3,
1174   IRF-5, and IRF-7 coordinately regulate the type I IFN response in myeloid dendritic cells
1175   downstream of MAVS signaling. PLoS Pathog. 2013;9(1):e1003118. Epub 2013/01/10. doi:
1176   10.1371/journal.ppat.1003118. PubMed PMID: 23300459; PubMed Central PMCID:
1177   PMCPMC3536698.
1178   32.   Osterlund PI, Pietila TE, Veckman V, Kotenko SV, Julkunen I. IFN regulatory factor
1179   family members differentially regulate the expression of type III IFN (IFN-lambda) genes. J
1180   Immunol. 2007;179(6):3434-42. Epub 2007/09/06. PubMed PMID: 17785777.
1181   33.   La Gruta NL, Kedzierska K, Stambas J, Doherty PC. A question of self-preservation:
1182   immunopathology in influenza virus infection. Immunol Cell Biol. 2007;85(2):85-92. Epub
1183   2007/01/11. doi: 10.1038/sj.icb.7100026. PubMed PMID: 17213831.
1184   34.   Liu Q, Zhou YH, Yang ZQ. The cytokine storm of severe influenza and development
1185   of immunomodulatory therapy. Cell Mol Immunol. 2016;13(1):3-10. doi:
1186   10.1038/cmi.2015.74. PubMed PMID: 26189369; PubMed Central PMCID:
1187   PMCPMC4711683.
1188   35.   Hutchinson EC. Influenza Virus. Trends Microbiol. 2018. doi:
1189   10.1016/j.tim.2018.05.013. PubMed PMID: 29909041.
1190   36.   van Tol S, Hage A, Giraldo MI, Bharaj P, Rajsbaum R. The TRIMendous Role of
1191   TRIMs in Virus-Host Interactions. Vaccines (Basel). 2017;5(3). doi:
1192   10.3390/vaccines5030023. PubMed PMID: 28829373; PubMed Central PMCID:
1193   PMCPMC5620554.
1194   37.   van Gent M, Sparrer KMJ, Gack MU. TRIM Proteins and Their Roles in Antiviral
1195   Host Defenses. Annu Rev Virol. 2018. doi: 10.1146/annurev-virology-092917-043323.
1196   PubMed PMID: 29949725.
1197   38.   Kawai T, Akira S. Regulation of innate immune signalling pathways by the tripartite
1198   motif (TRIM) family proteins. EMBO Mol Med. 2011;3(9):513-27. doi:
1199   10.1002/emmm.201100160. PubMed PMID: 21826793; PubMed Central PMCID:
1200   PMCPMC3377094.
1201   39.   Rajsbaum R, Garcia-Sastre A, Versteeg GA. TRIMmunity: the roles of the TRIM E3-
1202   ubiquitin ligase family in innate antiviral immunity. J Mol Biol. 2014;426(6):1265-84. doi:
1203   10.1016/j.jmb.2013.12.005. PubMed PMID: 24333484; PubMed Central PMCID:
1204   PMCPMC3945521.

1205   40.   Rajsbaum R, Stoye JP, O'Garra A. Type I interferon-dependent and -independent
1206   expression of tripartite motif proteins in immune cells. Eur J Immunol. 2008;38(3):619-30.
1207   doi: 10.1002/eji.200737916. PubMed PMID: 18286572.
1208   41.   Carthagena L, Bergamaschi A, Luna JM, David A, Uchil PD, Margottin-Goguet F, et
1209   al. Human TRIM gene expression in response to interferons. PLoS One. 2009;4(3):e4894.
1210   doi: 10.1371/journal.pone.0004894. PubMed PMID: 19290053; PubMed Central PMCID:
1211   PMCPMC2654144.
1212   42.   Versteeg GA, Rajsbaum R, Sanchez-Aparicio MT, Maestre AM, Valdiviezo J, Shi M,
1213   et al. The E3-ligase TRIM family of proteins regulates signaling pathways triggered by innate
1214   immune pattern-recognition receptors. Immunity. 2013;38(2):384-98. doi:
1215   10.1016/j.immuni.2012.11.013. PubMed PMID: 23438823; PubMed Central PMCID:
1216   PMCPMC3584420.
1217   43.   Uchil PD, Quinlan BD, Chan WT, Luna JM, Mothes W. TRIM E3 ligases interfere
1218   with early and late stages of the retroviral life cycle. PLoS Pathog. 2008;4(2):e16. doi:
1219   10.1371/journal.ppat.0040016. PubMed PMID: 18248090; PubMed Central PMCID:
1220   PMCPMC2222954.
1221   44.   Uchil PD, Hinz A, Siegel S, Coenen-Stass A, Pertel T, Luban J, et al. TRIM protein-
1222   mediated regulation of inflammatory and innate immune signaling and its association with
1223   antiretroviral activity. J Virol. 2013;87(1):257-72. doi: 10.1128/JVI.01804-12. PubMed
1224   PMID: 23077300; PubMed Central PMCID: PMCPMC3536418.
1225   45.   Yu S, Gao B, Duan Z, Xu W, Xiong S. Identification of tripartite motif-containing 22
1226   (TRIM22) as a novel NF-kappaB activator. Biochem Biophys Res Commun.
1227   2011;410(2):247-51. Epub 2011/06/10. doi: 10.1016/j.bbrc.2011.05.124. PubMed PMID:
1228   21651891.
1229   46.   Everett RD, Rechter S, Papior P, Tavalai N, Stamminger T, Orr A. PML contributes
1230   to a cellular mechanism of repression of herpes simplex virus type 1 infection that is
1231   inactivated by ICP0. J Virol. 2006;80(16):7995-8005. doi: 10.1128/JVI.00734-06. PubMed
1232   PMID: 16873256; PubMed Central PMCID: PMCPMC1563828.
1233   47.   Everett RD, Parada C, Gripon P, Sirma H, Orr A. Replication of ICP0-null mutant
1234   herpes simplex virus type 1 is restricted by both PML and Sp100. J Virol. 2008;82(6):2661-
1235   72. Epub 2007/12/28. doi: 10.1128/JVI.02308-07. PubMed PMID: 18160441; PubMed
1236   Central PMCID: PMCPMC2258993.
1237   48.   Sebastian S, Luban J. TRIM5alpha selectively binds a restriction-sensitive retroviral
1238   capsid. Retrovirology. 2005;2:40. doi: 10.1186/1742-4690-2-40. PubMed PMID: 15967037;
1239   PubMed Central PMCID: PMCPMC1166576.
1240   49.   Stremlau M, Perron M, Lee M, Li Y, Song B, Javanbakht H, et al. Specific
1241   recognition and accelerated uncoating of retroviral capsids by the TRIM5alpha restriction
1242   factor. Proc Natl Acad Sci U S A. 2006;103(14):5514-9. doi: 10.1073/pnas.0509996103.
1243   PubMed PMID: 16540544; PubMed Central PMCID: PMCPMC1459386.
1244   50.   Barr SD, Smiley JR, Bushman FD. The interferon response inhibits HIV particle
1245   production by induction of TRIM22. PLoS Pathog. 2008;4(2):e1000007. doi:
1246   10.1371/journal.ppat.1000007. PubMed PMID: 18389079; PubMed Central PMCID:
1247   PMCPMC2279259.
1248   51.   Gao B, Duan Z, Xu W, Xiong S. Tripartite motif-containing 22 inhibits the activity of
1249   hepatitis B virus core promoter, which is dependent on nuclear-located RING domain.
1250   Hepatology. 2009;50(2):424-33. doi: 10.1002/hep.23011. PubMed PMID: 19585648.
1251   52.   Yang C, Zhao X, Sun D, Yang L, Chong C, Pan Y, et al. Interferon alpha (IFNalpha)-
1252   induced TRIM22 interrupts HCV replication by ubiquitinating NS5A. Cell Mol Immunol.
1253   2016;13(1):94-102. doi: 10.1038/cmi.2014.131. PubMed PMID: 25683609; PubMed Central
1254   PMCID: PMCPMC4711679.

1255 53.   Eldin P, Papon L, Oteiza A, Brocchi E, Lawson TG, Mechti N. TRIM22 E3 ubiquitin
1256 ligase activity is required to mediate antiviral activity against encephalomyocarditis virus. J
1257 Gen Virol. 2009;90(Pt 3):536-45. doi: 10.1099/vir.0.006288-0. PubMed PMID: 19218198.
1258 54.   Hattlmann CJ, Kelly JN, Barr SD. TRIM22: A Diverse and Dynamic Antiviral
1259 Protein. Mol Biol Int. 2012;2012:153415. doi: 10.1155/2012/153415. PubMed PMID:
1260 22649727; PubMed Central PMCID: PMCPMC3356915.
1261 55.   Di Pietro A, Kajaste-Rudnitski A, Oteiza A, Nicora L, Towers GJ, Mechti N, et al.
1262 TRIM22 inhibits influenza A virus infection by targeting the viral nucleoprotein for
1263 degradation. J Virol. 2013;87(8):4523-33. doi: 10.1128/JVI.02548-12. PubMed PMID:
1264 23408607; PubMed Central PMCID: PMCPMC3624352.
1265 56.   Mo XY, Ma W, Zhang Y, Zhao H, Deng Y, Yuan W, et al. Microarray analyses of
1266 differentially expressed human genes and biological processes in ECV304 cells infected with
1267 rubella virus. J Med Virol. 2007;79(11):1783-91. doi: 10.1002/jmv.20942. PubMed PMID:
1268 17854033.
1269 57.   Vicenzi E, Poli G. The interferon-stimulated gene TRIM22: A double-edged sword in
1270 HIV-1 infection. Cytokine Growth Factor Rev. 2018;40:40-7. doi:
1271 10.1016/j.cytogfr.2018.02.001. PubMed PMID: 29650252.
1272 58.   Kajaste-Rudnitski A, Marelli SS, Pultrone C, Pertel T, Uchil PD, Mechti N, et al.
1273 TRIM22 inhibits HIV-1 transcription independently of its E3 ubiquitin ligase activity, Tat,
1274 and NF-kappaB-responsive long terminal repeat elements. J Virol. 2011;85(10):5183-96. doi:
1275 10.1128/JVI.02302-10. PubMed PMID: 21345949; PubMed Central PMCID:
1276 PMCPMC3126207.
1277 59.   Singh R, Gaiha G, Werner L, McKim K, Mlisana K, Luban J, et al. Association of
1278 TRIM22 with the type 1 interferon response and viral control during primary HIV-1
1279 infection. J Virol. 2011;85(1):208-16. doi: 10.1128/JVI.01810-10. PubMed PMID:
1280 20980524; PubMed Central PMCID: PMCPMC3014203.
1281 60.   Turrini F, Marelli S, Kajaste-Rudnitski A, Lusic M, Van Lint C, Das AT, et al. HIV-1
1282 transcriptional silencing caused by TRIM22 inhibition of Sp1 binding to the viral promoter.
1283 Retrovirology. 2015;12:104. doi: 10.1186/s12977-015-0230-0. PubMed PMID: 26683615;
1284 PubMed Central PMCID: PMCPMC4683785.
1285 61.   Pagani I, Di Pietro A, Oteiza A, Ghitti M, Mechti N, Naffakh N, et al. Mutations
1286 Conferring Increased Sensitivity to Tripartite Motif 22 Restriction Accumulated
1287 Progressively in the Nucleoprotein of Seasonal Influenza A (H1N1) Viruses between 1918
1288 and 2009. mSphere. 2018;3(2). doi: 10.1128/mSphere.00110-18. PubMed PMID: 29624498;
1289 PubMed Central PMCID: PMCPMC5885024.
1290 62.   Uhlen M, Fagerberg L, Hallstrom BM, Lindskog C, Oksvold P, Mardinoglu A, et al.
1291 Proteomics. Tissue-based map of the human proteome. Science. 2015;347(6220):1260419.
1292 doi: 10.1126/science.1260419. PubMed PMID: 25613900.
1293 63.   Uhlen M, Oksvold P, Fagerberg L, Lundberg E, Jonasson K, Forsberg M, et al.
1294 Towards a knowledge-based Human Protein Atlas. Nat Biotechnol. 2010;28(12):1248-50.
1295 doi: 10.1038/nbt1210-1248. PubMed PMID: 21139605.
1296 64.   Carithers LJ, Ardlie K, Barcus M, Branton PA, Britton A, Buia SA, et al. A Novel
1297 Approach to High-Quality Postmortem Tissue Procurement: The GTEx Project. Biopreserv
1298 Biobank. 2015;13(5):311-9. Epub 2015/10/21. doi: 10.1089/bio.2015.0032. PubMed PMID:
1299 26484571; PubMed Central PMCID: PMCPMC4675181.
1300 65.   Marriott AC, Dennis M, Kane JA, Gooch KE, Hatch G, Sharpe S, et al. Influenza A
1301 Virus Challenge Models in Cynomolgus Macaques Using the Authentic Inhaled Aerosol and
1302 Intra-Nasal Routes of Infection. PLoS One. 2016;11(6):e0157887. doi:
1303 10.1371/journal.pone.0157887. PubMed PMID: 27311020; PubMed Central PMCID:
1304 PMCPMC4911124.

1305 66. Stewart CE, Randall RE, Adamson CS. Inhibitors of the interferon response enhance
1306 virus replication in vitro. PLoS One. 2014;9(11):e112014. Epub 2014/11/13. doi:
1307 10.1371/journal.pone.0112014. PubMed PMID: 25390891; PubMed Central PMCID:
1308 PMCPMC4229124.
1309 67. Shaw AE, Hughes J, Gu Q, Behdenna A, Singer JB, Dennis T, et al. Fundamental
1310 properties of the mammalian innate immune system revealed by multispecies comparison of
1311 type I interferon responses. PLoS Biol. 2017;15(12):e2004086. Epub 2017/12/19. doi:
1312 10.1371/journal.pbio.2004086. PubMed PMID: 29253856; PubMed Central PMCID:
1313 PMCPMC5747502.
1314 68. Tovey MG, Streuli M, Gresser I, Gugenheim J, Blanchard B, Guymarho J, et al.
1315 Interferon messenger RNA is produced constitutively in the organs of normal individuals.
1316 Proc Natl Acad Sci U S A. 1987;84(14):5038-42. Epub 1987/07/01. doi:
1317 10.1073/pnas.84.14.5038. PubMed PMID: 3110782; PubMed Central PMCID:
1318 PMCPMC305242.
1319 69. Gough DJ, Messina NL, Clarke CJ, Johnstone RW, Levy DE. Constitutive type I
1320 interferon modulates homeostatic balance through tonic signaling. Immunity.
1321 2012;36(2):166-74. Epub 2012/03/01. doi: 10.1016/j.immuni.2012.01.011. PubMed PMID:
1322 22365663; PubMed Central PMCID: PMCPMC3294371.
1323 70. Villalon-Letelier F, Brooks AG, Saunders PM, Londrigan SL, Reading PC. Host Cell
1324 Restriction Factors that Limit Influenza A Infection. Viruses. 2017;9(12). Epub 2017/12/08.
1325 doi: 10.3390/v9120376. PubMed PMID: 29215570; PubMed Central PMCID:
1326 PMCPMC5744151.
1327 71. Shim JM, Kim J, Tenson T, Min JY, Kainov DE. Influenza Virus Infection, Interferon
1328 Response, Viral Counter-Response, and Apoptosis. Viruses. 2017;9(8). Epub 2017/08/15.
1329 doi: 10.3390/v9080223. PubMed PMID: 28805681; PubMed Central PMCID:
1330 PMCPMC5580480.
1331 72. Szklarczyk D, Gable AL, Lyon D, Junge A, Wyder S, Huerta-Cepas J, et al. STRING
1332 v11: protein-protein association networks with increased coverage, supporting functional
1333 discovery in genome-wide experimental datasets. Nucleic Acids Res. 2019;47(D1):D607-
1334 D13. Epub 2018/11/27. doi: 10.1093/nar/gky1131. PubMed PMID: 30476243; PubMed
1335 Central PMCID: PMCPMC6323986.
1336 73. Obad S, Brunnstrom H, Vallon-Christersson J, Borg A, Drott K, Gullberg U. Staf50 is
1337 a novel p53 target gene conferring reduced clonogenic growth of leukemic U-937 cells.
1338 Oncogene. 2004;23(23):4050-9. doi: 10.1038/sj.onc.1207524. PubMed PMID: 15064739.
1339 74. Ghandi M, Huang FW, Jane-Valbuena J, Kryukov GV, Lo CC, McDonald ER, 3rd, et
1340 al. Next-generation characterization of the Cancer Cell Line Encyclopedia. Nature. 2019.
1341 Epub 2019/05/10. doi: 10.1038/s41586-019-1186-3. PubMed PMID: 31068700.
1342 75. Barretina J, Caponigro G, Stransky N, Venkatesan K, Margolin AA, Kim S, et al. The
1343 Cancer Cell Line Encyclopedia enables predictive modelling of anticancer drug sensitivity.
1344 Nature. 2012;483(7391):603-7. Epub 2012/03/31. doi: 10.1038/nature11003. PubMed PMID:
1345 22460905; PubMed Central PMCID: PMCPMC3320027.
1346 76. Frishberg A, Peshes-Yaloz N, Cohn O, Rosentul D, Steuerman Y, Valadarsky L, et al.
1347 Cell composition analysis of bulk genomics using single-cell data. Nat Methods.
1348 2019;16(4):327-32. Epub 2019/03/20. doi: 10.1038/s41592-019-0355-5. PubMed PMID:
1349 30886410; PubMed Central PMCID: PMCPMC6443043.
1350 77. Woo SR, Corrales L, Gajewski TF. Innate immune recognition of cancer. Annu Rev
1351 Immunol. 2015;33:445-74. Epub 2015/01/27. doi: 10.1146/annurev-immunol-032414-
1352 112043. PubMed PMID: 25622193.
1353 78. Corrales L, Matson V, Flood B, Spranger S, Gajewski TF. Innate immune signaling
1354 and regulation in cancer immunotherapy. Cell Res. 2017;27(1):96-108. Epub 2016/12/17.

doi: 10.1038/cr.2016.149. PubMed PMID: 27981969; PubMed Central PMCID: PMCPMC5223230.

79.   Mehle A, Doudna JA. A host of factors regulating influenza virus replication. Viruses. 2010;2(2):566-73. Epub 2010/02/01. doi: 10.3390/v2020566. PubMed PMID: 21994648; PubMed Central PMCID: PMCPMC3185602.

80.   Watanabe T, Watanabe S, Kawaoka Y. Cellular networks involved in the influenza virus life cycle. Cell Host Microbe. 2010;7(6):427-39. Epub 2010/06/15. doi: 10.1016/j.chom.2010.05.008. PubMed PMID: 20542247; PubMed Central PMCID: PMCPMC3167038.

81.   Hao L, He Q, Wang Z, Craven M, Newton MA, Ahlquist P. Limited agreement of independent RNAi screens for virus-required host genes owes more to false-negative than false-positive factors. PLoS Comput Biol. 2013;9(9):e1003235. Epub 2013/09/27. doi: 10.1371/journal.pcbi.1003235. PubMed PMID: 24068911; PubMed Central PMCID: PMCPMC3777922.

82.   McFarlane S, Orr A, Roberts APE, Conn KL, Iliev V, Loney C, et al. The histone chaperone HIRA promotes the induction of host innate immune defences in response to HSV-1 infection. PLoS Pathog. 2019;15(3):e1007667. Epub 2019/03/23. doi: 10.1371/journal.ppat.1007667. PubMed PMID: 30901352.

83.   Bocci V. Is interferon produced in physiologic conditions? Med Hypotheses. 1980;6(7):735-45. Epub 1980/07/01. PubMed PMID: 6157081.

84.   Gough DJ, Messina NL, Hii L, Gould JA, Sabapathy K, Robertson AP, et al. Functional crosstalk between type I and II interferon through the regulated expression of STAT1. PLoS Biol. 2010;8(4):e1000361. Epub 2010/05/04. doi: 10.1371/journal.pbio.1000361. PubMed PMID: 20436908; PubMed Central PMCID: PMCPMC2860501.

85.   Mostafavi S, Yoshida H, Moodley D, LeBoite H, Rothamel K, Raj T, et al. Parsing the Interferon Transcriptional Network and Its Disease Associations. Cell. 2016;164(3):564-78. Epub 2016/01/30. doi: 10.1016/j.cell.2015.12.032. PubMed PMID: 26824662; PubMed Central PMCID: PMCPMC4743492.

86.   Kamada R, Yang W, Zhang Y, Patel MC, Yang Y, Ouda R, et al. Interferon stimulation creates chromatin marks and establishes transcriptional memory. Proc Natl Acad Sci U S A. 2018;115(39):E9162-E71. Epub 2018/09/12. doi: 10.1073/pnas.1720930115. PubMed PMID: 30201712; PubMed Central PMCID: PMCPMC6166839.

87.   Everitt AR, Clare S, Pertel T, John SP, Wash RS, Smith SE, et al. IFITM3 restricts the morbidity and mortality associated with influenza. Nature. 2012;484(7395):519-23. Epub 2012/03/27. doi: 10.1038/nature10921. PubMed PMID: 22446628; PubMed Central PMCID: PMCPMC3648786.

88.   Wu X, Dao Thi VL, Huang Y, Billerbeck E, Saha D, Hoffmann HH, et al. Intrinsic Immunity Shapes Viral Resistance of Stem Cells. Cell. 2018;172(3):423-38 e25. Epub 2017/12/19. doi: 10.1016/j.cell.2017.11.018. PubMed PMID: 29249360; PubMed Central PMCID: PMCPMC5786493.

89.   Turnbull ML, Wise HM, Nicol MQ, Smith N, Dunfee RL, Beard PM, et al. Role of the B Allele of Influenza A Virus Segment 8 in Setting Mammalian Host Range and Pathogenicity. J Virol. 2016;90(20):9263-84. doi: 10.1128/JVI.01205-16. PubMed PMID: 27489273; PubMed Central PMCID: PMCPMC5044859.

90.   Akram KM, Moyo NA, Leeming GH, Bingle L, Jasim S, Hussain S, et al. An innate defense peptide BPIFA1/SPLUNC1 restricts influenza A virus infection. Mucosal Immunol. 2018;11(1):71-81. doi: 10.1038/mi.2017.45. PubMed PMID: 28513596.

91.   Leeming GH, Kipar A, Hughes DJ, Bingle L, Bennett E, Moyo NA, et al. Gammaherpesvirus infection modulates the temporal and spatial expression of SCGB1A1

1405   (CCSP) and BPIFA1 (SPLUNC1) in the respiratory tract. Lab Invest. 2015;95(6):610-24.
1406   doi: 10.1038/labinvest.2014.162. PubMed PMID: 25531566; PubMed Central PMCID:
1407   PMCPMC4450743.
1408   92.   Smith MC, Goddard ET, Perusina Lanfranca M, Davido DJ. hTERT extends the life
1409   of human fibroblasts without compromising type I interferon signaling. PLoS One.
1410   2013;8(3):e58233. doi: 10.1371/journal.pone.0058233. PubMed PMID: 23472163; PubMed
1411   Central PMCID: PMCPMC3589264.
1412   93.   Ramirez RD, Sheridan S, Girard L, Sato M, Kim Y, Pollack J, et al. Immortalization
1413   of human bronchial epithelial cells in the absence of viral oncoproteins. Cancer Res.
1414   2004;64(24):9027-34. Epub 2004/12/18. doi: 10.1158/0008-5472.CAN-04-3703. PubMed
1415   PMID: 15604268.
1416   94.   Conn KL, Wasson P, McFarlane S, Tong L, Brown JR, Grant KG, et al. Novel Role
1417   for Protein Inhibitor of Activated STAT 4 (PIAS4) in the Restriction of Herpes Simplex
1418   Virus 1 by the Cellular Intrinsic Antiviral Immune Response. J Virol. 2016;90(9):4807-26.
1419   doi: 10.1128/JVI.03055-15. PubMed PMID: 26937035; PubMed Central PMCID:
1420   PMCPMC4836348.
1421   95.   Vester D, Lagoda A, Hoffmann D, Seitz C, Heldt S, Bettenbrock K, et al. Real-time
1422   RT-qPCR assay for the analysis of human influenza A virus transcription and replication
1423   dynamics. J Virol Methods. 2010;168(1-2):63-71. doi: 10.1016/j.jviromet.2010.04.017.
1424   PubMed PMID: 20433869.
1425   96.   Fodor E, Crow M, Mingay LJ, Deng T, Sharps J, Fechter P, et al. A single amino acid
1426   mutation in the PA subunit of the influenza virus RNA polymerase inhibits endonucleolytic
1427   cleavage of capped RNAs. J Virol. 2002;76(18):8989-9001. PubMed PMID: 12186883;
1428   PubMed Central PMCID: PMCPMC136441.
1429   97.   Benfield CT, Lyall JW, Kochs G, Tiley LS. Asparagine 631 variants of the chicken
1430   Mx protein do not inhibit influenza virus replication in primary chicken embryo fibroblasts or
1431   in vitro surrogate assays. J Virol. 2008;82(15):7533-9. doi: 10.1128/JVI.00185-08. PubMed
1432   PMID: 18508886; PubMed Central PMCID: PMCPMC2493316.

1433

Fig 1

Fig 2

Fig 3

A.

Rel. mRNA levels (No IFN)

Ruxo (μM):	0	0	0.25	1	4	16
IFN-β:	−	+	+	+	+	+

Legend: *Mx1*, *ISG15*

B.

● shCtrl ● shTRIM22

Rel. IAV (WSN) PFE (shTRIM22/shCtrl)

ns

Ruxo: (4μM)	−	−	+	+

Fig 4

A.

	DAPI	TRIM22	NP
shCtrl			
shTRIM22			

IAV (PR8; MOI 0.05 FFU/cell)

B.

● human IAV   ● avian IAV

Rel. NP positive cells (shTRIM22/shCtrl)

IAV strain

PR8 (H1N1)   WSN (H1N1)   Udorn (H3N2)   Duck (H5N3)   Chicken (H7N1)

Fig 5

Fig 6

A. ISG expression (200 genes; every 2nd labelled)

B. Top 50 constitutively expressed ISGs (lung)

C.

D. ISG expression (all tissues)

E.

F.

IFN related receptors   IFN related cytokines

G.

Fig 7

Fig 8

A.

514 downregulated genes (total): 93 (18.09%) immune-related

661 downregulated genes (total): 115 (17.39%) immune-related

656 downregulated genes (total): 108 (16.46%) immune-related

B. Differentially downregulated immune genes (174 unique genes; every 2nd labelled)

Core (45 genes)   Shared (50 genes)   Unique (79 genes)

log2 TPM   -6.6   0   12
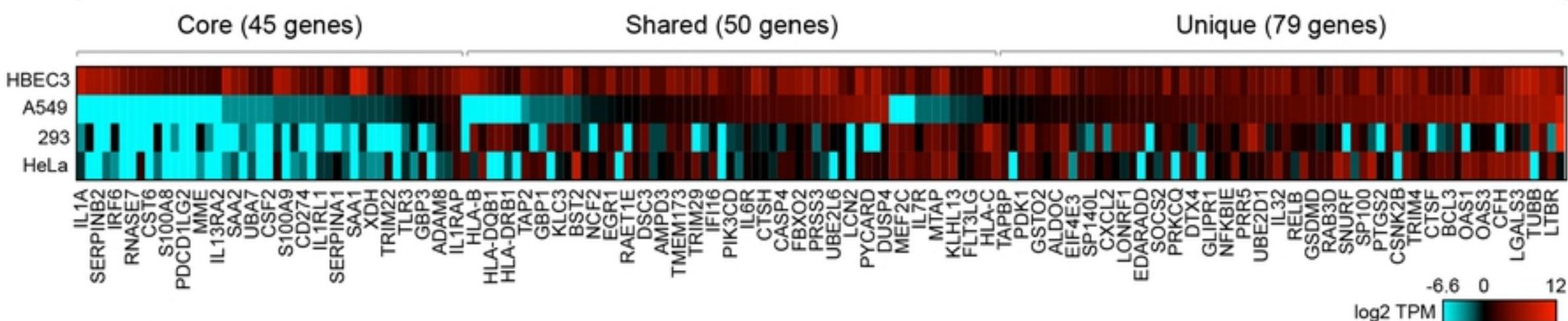
C.
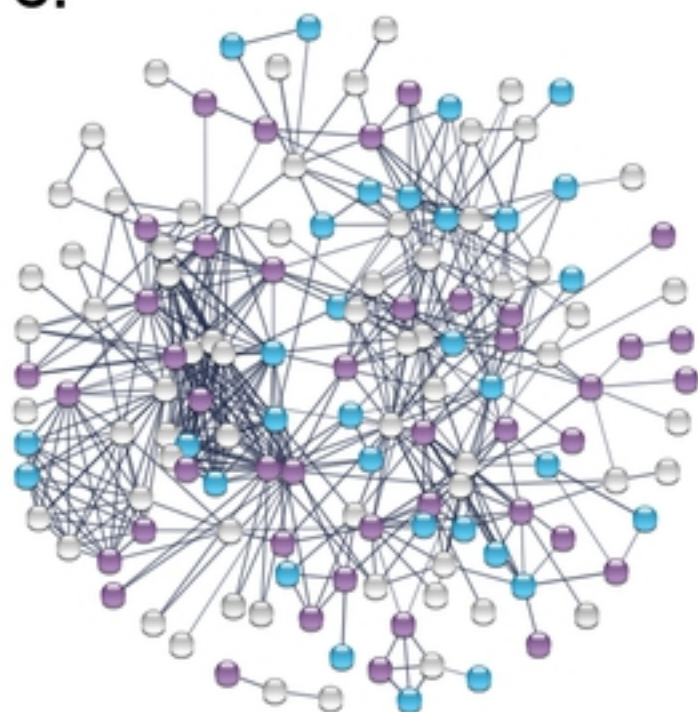
Biological Process (GO)

Pathway Description	Count in gene set	FDR
immune response	108 of 1560	2.64E-31
immune system process	120 of 2370	1.74E-29
defense response	86 of 1234	1.84E-24
response to cytokine	69 of 655	7.68E-19
cellular response to cytokine stimulus	78 of 1035	7.89E-19

KEGG

Pathway Description	Count in gene set	FDR
NOD-like receptor signaling pathway	18 of 166	9.3E-12
Influenza A	17 of 168	5.3E-11
IL-17 signaling pathway	14 of 92	5.3E-11
Cytokine-cytokine receptor interaction	20 of 263	5.3E-11
Natural killer cell mediated cytotoxicity	14 of 124	8.28E-10

Downregulated immune system network: Connected (141 of 174 genes); No connection (33 of 174 genes); PPI enrichment: *P* < 1.0e-16; Core (●), Shared (●), Unique (○)
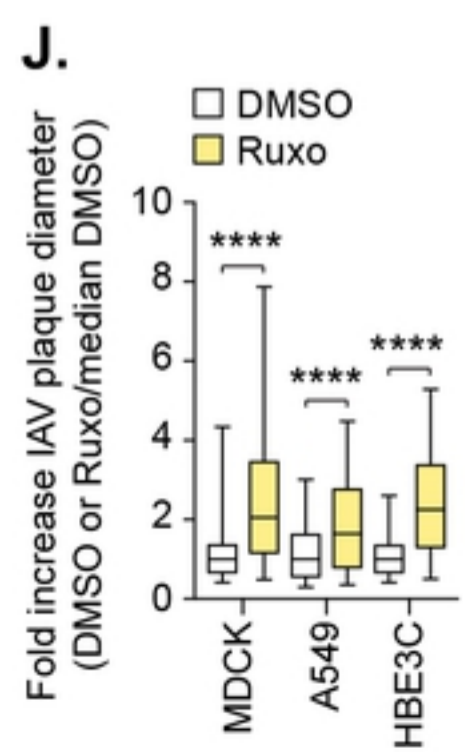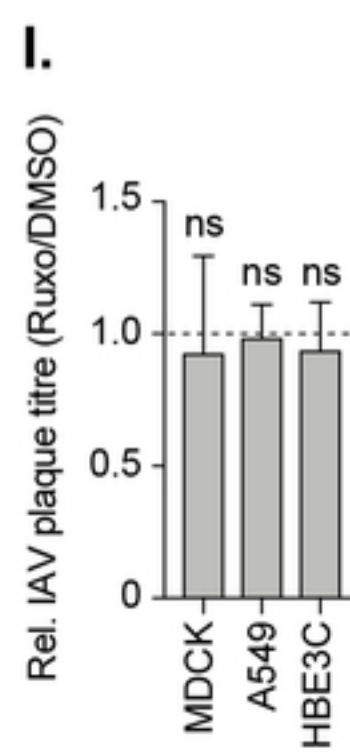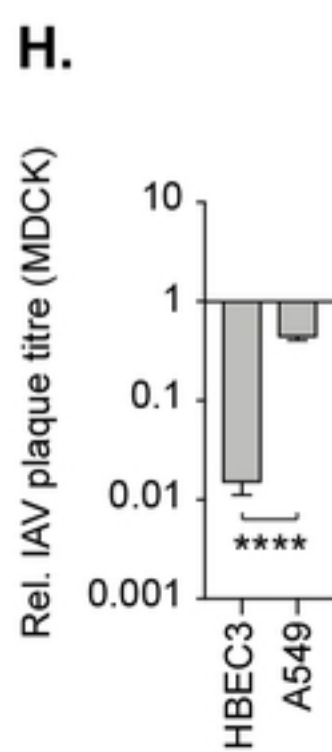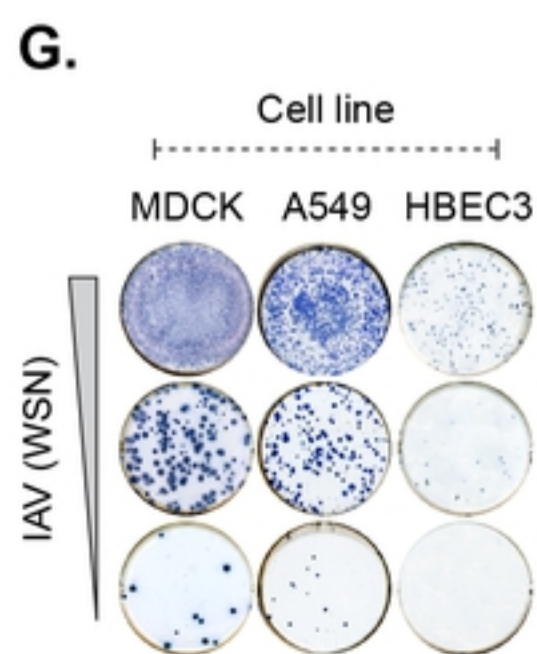
Fig 9

A.

IAV immuno-regulators (184 genes; every 2nd labelled)

log2 TPM: -6.6 — 0 — 12

B.

downregulated IAV immuno-regulators (HBEC3 ≥ 5-fold; ≥ 3 TPM)

log2 TPM: -6.6 — 0 — 11

C.

IIAV immuno-regulator expression (log2 TPM)

HBEC3, A549 (**), HEK 293 (****), HeLa (**), Lung (GTEx) (ns)

D.

Downregulated KEGG IAV network
Connected (29 of 39 genes)
No connection (10 of 39 genes)
PPI enrichment: $P < 1.0e-16$
Core (●); Shared (●); Unique (○)

E.

A549 / HBEC3

UBA7, GBP1, TRIM22, Actin — set 1
IFIH1, TRIM22, Actin — set 2
TLR3, TRIM22, IFITM1, Actin — set 3

F.

Rel. protein levels (HBEC3) — HBEC3 (dashed), A549

UBA7 (**), TRIM22 (****), IFITM1 (****), GBP1 (****), IFIH1 (**), TLR3 (**)

G.

Cell line: MDCK, A549, HBEC3
IAV (WSN)

H.

Rel. IAV plaque titre (MDCK) — HBEC3, A549 (****)

I.

Rel. IAV plaque titre (Ruxo/DMSO) — MDCK (ns), A549 (ns), HBE3C (ns)

J.

Fold increase IAV plaque diameter (DMSO or Ruxo/median DMSO) — DMSO, Ruxo
MDCK (****), A549 (****), HBE3C (****)

Fig 10